5. G. Pfeffer, K. Majamaa, D. M. Turnbull, D. Thorburn, P. F. Chinnery, *Cochrane Database Syst. Rev.* **4**, CD004426 (2012).
6. N. J. Lake, M. J. Bird, P. Isohanni, A. Paetau, *J. Neuropathol. Exp. Neurol.* **74**, 482–492 (2015).
7. G. S. Gorman *et al.*, *Ann. Neurol.* **77**, 753–759 (2015).
8. S. Parikh *et al.*, *Genet. Med.* **17**, 689–701 (2015).
9. R. H. Haas *et al.*, *Pediatrics* **120**, 1326–1333 (2007).
10. O. Shalem *et al.*, *Science* **343**, 84–87 (2014).
11. T. Wang, J. J. Wei, D. M. Sabatini, E. S. Lander, *Science* **343**, 80–84 (2014).
12. M. P. King, G. Attardi, *Science* **246**, 500–503 (1989).
13. S. E. Calvo, K. R. Clauser, V. K. Mootha, *Nucleic Acids Res.* **44**, D1251–D1257 (2016).
14. M. Ohh *et al.*, *Nat. Cell Biol.* **2**, 423–427 (2000).
15. C. M. Robinson, M. Ohh, *FEBS Lett.* **588**, 2704–2711 (2014).
16. G. L. Wang, B. H. Jiang, E. A. Rue, G. L. Semenza, *Proc. Natl. Acad. Sci. U.S.A.* **92**, 5510–5514 (1995).
17. A. J. Majmundar, W. J. Wong, M. C. Simon, *Mol. Cell* **40**, 294–309 (2010).
18. M. Ivan *et al.*, *Proc. Natl. Acad. Sci. U.S.A.* **99**, 13459–13464 (2002).
19. O. Iliopoulos, A. P. Levy, C. Jiang, W. G. Kaelin Jr., M. A. Goldberg, *Proc. Natl. Acad. Sci. U.S.A.* **93**, 10595–10599 (1996).
20. P. H. Maxwell *et al.*, *Nature* **399**, 271–275 (1999).
21. D. L. Buckley *et al.*, *J. Am. Chem. Soc.* **134**, 4465–4468 (2012).
22. M. H. Rabinowitz, *J. Med. Chem.* **56**, 9369–9402 (2013).
23. N. S. Chandel *et al.*, *Proc. Natl. Acad. Sci. U.S.A.* **95**, 11715–11720 (1998).
24. Y. L. Chua *et al.*, *J. Biol. Chem.* **285**, 31277–31284 (2010).
25. I. Papandreou, R. A. Cairns, L. Fontana, A. L. Lim, N. C. Denko, *Cell Metab.* **3**, 187–197 (2006).
26. D. Tello *et al.*, *Cell Metab.* **14**, 768–779 (2011).
27. J. W. Kim, I. Tchernyshyov, G. L. Semenza, C. V. Dang, *Cell Metab.* **3**, 177–185 (2006).
28. M. C. Simon, *Cell Metab.* **3**, 150–151 (2006).
29. E. van Rooijen *et al.*, *Blood* **113**, 6449–6460 (2009).
30. B. R. Pinho *et al.*, *Br. J. Pharmacol.* **169**, 1072–1090 (2013).
31. K. D. Stackley, C. C. Beeson, J. J. Rahn, S. S. Chan, *PLOS One* **6**, e25652 (2011).
32. J. M. Harris *et al.*, *Blood* **121**, 2483–2493 (2013).
33. K. Santhakumar *et al.*, *Cancer Res.* **72**, 4017–4027 (2012).
34. R. Chowdhury *et al.*, *ACS Chem. Biol.* **8**, 1488–1496 (2013).
35. S. E. Kruse *et al.*, *Cell Metab.* **7**, 312–320 (2008).
36. I. G. Pawson, *Proc. R. Soc. London Ser. B* **194**, 83–98 (1976).
37. J. Caston, N. Jones, T. Stelz, *Neurobiol. Learn. Mem.* **64**, 195–202 (1995).
38. A. Quintana, S. E. Kruse, R. P. Kapur, E. Sanz, R. D. Palmiter, *Proc. Natl. Acad. Sci. U.S.A.* **107**, 10996–11001 (2010).
39. J. Thompson Legault *et al.*, *Cell Rep.* **13**, 981–989 (2015).
40. R. S. Balaban, S. Nemoto, T. Finkel, *Cell* **120**, 483–495 (2005).

ACKNOWLEDGMENTS

We thank W. Kaelin Jr. and members of the Mootha lab for valuable feedback; R. Sharma, M. Ferrari, A. Rogers, and the MGH animal facility for assistance with experiments; and F. van Eeden for Tg(*phd3::EGFP*) zebrafish. I.H.J. is supported by the Department of Energy Computational Science Graduate Fellowship Program (grant DE-FG02-97ER25308). N.E.S. is supported by the National Institutes of Health (NIH) through a NHGRI Pathway to Independence Award (K99-HG008171) and a postdoctoral fellowship from the Simons Center for the Social Brain at the Massachusetts Institute of Technology. F.Z. is supported by NIH through NIMH (grants 5DP1-MH100706 and 1R01-MH110049) and NIDDK (grant 5R01DK097768-03); a Waterman Award from NSF; the New York Stem Cell, Simons, Paul G. Allen Family, and Vallee Foundations; and B. Metcalfe. F.Z. is a New York Stem Cell Foundation Robertson Investigator. W.G. is supported by NIH grants R01DK090311 and R24OD017870 and is a Pew Scholar in the Biomedical Sciences. This work was supported by a gift from the Marriott Mitochondrial Disorders Research Fund (V.K.M.) and a gift in memory of Daniel Garland (V.K.M.). V.K.M. is an Investigator of the Howard Hughes Medical Institute. V.K.M. is a founder of and paid scientific advisor for Raze Therapeutics. W.G. is a paid consultant for FATE Therapeutics. F.Z. is a founder of and a scientific advisor for Editas Medicine and a scientific advisor for Horizon Discovery. V.K.M., I.H.J., L.Z., and W.M.Z. are listed as inventors on a patent application filed by Massachusetts General Hospital related to technology reported in this paper on the use of hypoxia and the hypoxia response in the treatment of mitochondrial dysfunction. F.Z., O.S., and N.E.S. are listed as inventors on a patent application (PCT/US2013/074800) filed by The Broad Institute/MIT related to the genome-scale CRISPR knockout screening technology used in this study. The CRISPR knockout library is available through a Uniform Biological Materials Transfer Agreement from Addgene. The *Ndufs4* KO mice were a kind gift of R. Palmiter and are available under a materials transfer agreement with the University of Washington, Seattle.

SUPPLEMENTARY MATERIALS

www.sciencemag.org/content/352/6281/54/suppl/DC1
Materials and Methods
Figs. S1 to S10
Tables S1 and S2
References (*41*–*44*)

14 August 2015; accepted 9 February 2016
Published online 25 February 2016
10.1126/science.aad9642

FLOW CHEMISTRY

On-demand continuous-flow production of pharmaceuticals in a compact, reconfigurable system

Andrea Adamo,[1] Rachel L. Beingessner,[2] Mohsen Behnam,[1]* Jie Chen,[1] Timothy F. Jamison,[2]† Klavs F. Jensen,[1]† Jean-Christophe M. Monbaliu,[1]‡ Allan S. Myerson,[1]† Eve M. Revalor,[1]§ David R. Snead,[2]|| Torsten Stelzer,[1]¶ Nopphon Weeranoppanant,[1] Shin Yee Wong,[1]# Ping Zhang[2]

Pharmaceutical manufacturing typically uses batch processing at multiple locations. Disadvantages of this approach include long production times and the potential for supply chain disruptions. As a preliminary demonstration of an alternative approach, we report here the continuous-flow synthesis and formulation of active pharmaceutical ingredients in a compact, reconfigurable manufacturing platform. Continuous end-to-end synthesis in the refrigerator-sized [1.0 meter (width) × 0.7 meter (length) × 1.8 meter (height)] system produces sufficient quantities per day to supply hundreds to thousands of oral or topical liquid doses of diphenhydramine hydrochloride, lidocaine hydrochloride, diazepam, and fluoxetine hydrochloride that meet U.S. Pharmacopeia standards. Underlying this flexible plug-and-play approach are substantial enabling advances in continuous-flow synthesis, complex multistep sequence telescoping, reaction engineering equipment, and real-time formulation.

Whereas manufacturing of automobiles, electronics, petrochemicals, polymers, and food use an assembly-line and/or continuous, steady-state strategy, pharmaceutical synthesis remains one of the last industrial processes to apply a noncontinuous or "batch" approach. Moreover, pharmaceutical companies generally assemble the active pharmaceutical ingredient (API) using molecular fragments obtained from different sources, with the final synthesis steps done at the company location. The API is then often mixed with excipients and formulated in the final drug product form at a separate plant. As a result, production of a finished dosage form can require up to a total of 12 months, with large inventories of intermediates at several stages. This enormous space-time demand is one of a myriad of reasons that has led to increased interest in continuous manufacturing of APIs and drug products, as well as in the development of integrated processes that would manufacture the drug product from raw materials in a single end-to-end process (*1*–*5*).

Another major challenge facing the pharmaceutical industry is drug shortages; the U.S. Food and Drug Administration (FDA) has reported well over 200 cases per year during 2011–2014 (*6*). The root causes of these shortages often trace back to factors reflective of the limitations of batchwise manufacturing, such as variations in quality control and supply chain interruption. Moreover, the small number of suppliers for any particular medicine further exacerbates the challenges faced by batchwise manufacturing to respond to sudden changes in demand or need,

[1]Department of Chemical Engineering, Massachusetts Institute of Technology, 77 Massachusetts Avenue, Cambridge, MA 02139, USA. [2]Department of Chemistry, Massachusetts Institute of Technology, 77 Massachusetts Avenue, Cambridge, MA 02139, USA.
*Present address: Nuvera Fuel Cells, 129 Concord Road, Billerica, MA 01821, USA. **†Corresponding author. E-mail: tfj@mit.edu (T.F.J); kfjensen@mit.edu (K.F.J); myerson@mit.edu (A.S.M)**
‡Present address: Department of Chemistry, University of Liège, Quartier Agora, Allée du six Août 13, B-4000 Liège (Sart Tilman), Belgium. §Present address: Department of Chemical and Biomolecular Engineering, Faculty of Medicine, Dentistry and Health Sciences, University of Melbourne, 3010 VIC, Australia. ||Present address: Georgia-Pacific Chemicals, 2883 Miller Road, Decatur, GA 30312, USA. ¶Present address: Department of Pharmaceutical Sciences, University of Puerto Rico, Medical Sciences Campus, San Juan, PR 00936, USA. #Present address: Chemical Engineering and Food Technology Cluster, Singapore Institute of Technology, 10 Dover Drive, Singapore 138683. **Present address: Novartis Institute of Biomedical Research, 250 Massachusetts Avenue, Cambridge, MA 02139, USA.

Downloaded from on March 31, 2016

such as in epidemic or pandemic instances of influenza outbreak.

To address the above issues, we have developed a continuous manufacturing platform that combines both synthesis and final drug product formulation into a single, highly compact unit (Fig. 1). The utilization of continuous flow (*7*–*9*) within the system enables efficient heat and mass transfer, as well as process intensification (*10*) and automation. Over the past several years, the merits of flow chemistry in streamlining synthesis (*11*) have been successfully demonstrated in the preparation of many individual high-profile APIs (*12*, *13*), including artemisinin (*14*), imatinib (*15*), efavirenz (*16*), nabumetone (*17*), rufinamide (*18*), pregabalin (*19*), and (*E*/*Z*)-tamoxifen (*20*).

Work with colleagues at the Massachusetts Institute of Technology (MIT) on end-to-end, continuous manufacturing of a single API, aliskiren hemifumarate, in a shipping container–sized unit (*21*) enabled us to identify critical steps in on-demand manufacturing of pharmaceuticals. Specifically, we chose to address challenges in reconfiguration for multiple synthesis of multiple compounds, tight integration of process streams for reduced footprint, innovations in chemical reaction and purification equipment, and compact systems for crystallization and formulation. As a result, the current system is ~1/40 the size and reconfigurable, in order to enable the on-demand synthesis and formulation of not just one, but many drug products. With the necessary regulatory approvals, this proof-of-principle system could enable a gradual phase-in of pharmaceutical production in response to demand. Reproduction of the system would be simpler and less costly to operate than a full batch plant and so could produce pharmaceuticals only needed for small patient populations or to meet humanitarian needs. It could be particularly advantageous for drugs with a short shelf life. Furthermore, the ability to manufacture the active ingredient on demand could reduce formulation complexity relative to tablets needing yearlong stability.

The flexible, plug-and-play refrigerator-sized platform (Fig. 1) [1.0 m (width) × 0.7 m (length) × 1.8 m (height), ~100 kg] is capable of complex multistep synthesis, multiple in-line purifications, postsynthesis work-up and handling, semibatch crystallization, real-time process monitoring, and ultimately formulation of high-purity drug products. To demonstrate its capabilities, we produced, from raw materials, sufficient quantities to supply hundreds to thousands of consumable oral or topical liquid doses per day of four different pharmaceuticals: diphenhydramine hydrochloride (**1**), lidocaine hydrochloride (**2**), diazepam (**3**), and fluoxetine hydrochloride (**4**) (Fig. 2) (*22*). The latter API, fluoxetine hydrochloride (**4**), was synthesized as a racemic mixture, as approved by the FDA. These generic molecules from different drug classes have differing chemical structures and synthesis routes, thus challenging the capabilities and exploring the technical limits of the continuous-flow system. Moreover, they are drugs commonly found in a chief medic's toolkit. Diphenhydramine hydrochloride (**1**), for example, well known by the trade name Benadryl, is an ethanolamine-based antihistamine used to treat the common cold,

Fig. 1. Reconfigurable system for continuous production and formulation of APIs. (**A**) Labeled photograph of the stack of upstream synthesis modules. (**B**) Labeled photograph of the downstream purification and formulation modules. (**C**) Close-up examples of upstream units; PFA tube flow reactors in an aluminum shell for heating (left) and membrane surface tension–based separation units (right). (**D**) Images of some of the main components in the downstream unit including the (a) buffer tank, (b) precipitation tank, (c) filtration unit, (d) crystallization unit, (e) filtration unit, (f) formulation tank, (g) solution holding tank, and (h) formulated API. Details are in the supplementary text.

lessen symptoms of allergies, and act as a mild sleep aid. Lidocaine hydrochloride (**2**), alternatively, is a common local anesthetic and class-1b antiarrhythmic drug. Diazepam (**3**), also known as Valium, is a central nervous system depressant. Finally, fluoxetine hydrochloride (**4**) is a widely used antidepressant recognized by its trade names Prozac and Sarafem.

As shown in Figs. 3 to 5, the synthesis of each API utilizes simple starting materials and reagents readily available from commercial suppliers and highlighted advantages that flow chemistry offers relative to batch synthesis. Synthetic schemes were first developed in flow on a microliter scale before translating to the platform. The reactions leverage quick exposure at elevated temperatures (130° to 180°C) and pressures (~1.7 MPa) in controlled environments to enable faster reactions with low impurity profiles and reduce total synthesis times from hours to minutes. Reagents were in high concentrations, close to saturation, and in some cases even neat, which ensured high productivity while reducing waste and solvent amounts. This is in contrast to batch conditions that use lower concentrations, as solvents often also serve as a heat transfer medium. Moreover, in the flow system, reaction and purification occurred at the same time at different locations within the same uninterrupted reactor network. In batch, each of the operations would be physically and temporally disconnected and would have much larger time, space, and workforce requirements, hence drastically increasing the global footprint and decreasing the global output of a given process.

Assembly of the platform

The system consists of reconfigurable upstream and downstream units (Fig. 1) that, despite having many complex operations, can be managed easily by an individual user. This is unlike typical batch manufacturing, which requires many operators to oversee multiple large-scale reactors and tanks with volumes on the order of thousands of liters and the transport and formulation of the final API in a separate processing plant (*23*). As shown in Fig. 1A, the upstream unit houses reaction-based equipment for producing APIs (e.g., feeds, pumps, reactors, separators, and pressure regulators) and has a maximum power requirement of 1.5 kW, which is mainly consumed by heating the reactors and operating the pumps. The backside (in Fig. 1A), alternatively, represents the downstream unit (Fig. 1B) dedicated to purification and formulation of the drug product (e.g., tanks to precipitate the crude API from reaction mixtures, crystallizers, and filters) (Fig. 1D). Temperature, pressure, flow, and level sensors

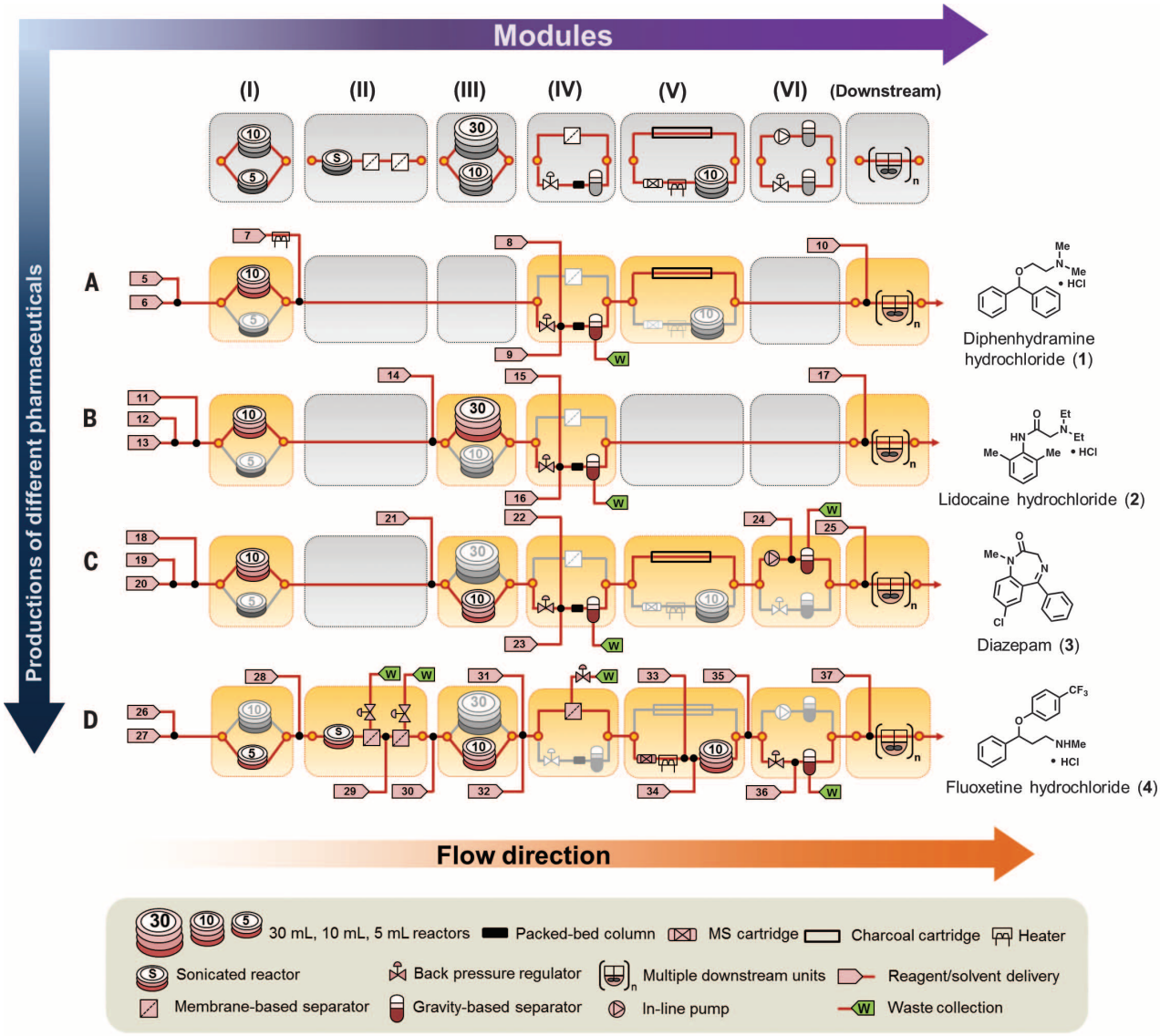

Fig. 2. Reconfigurable modules and flowcharts for API synthesis. (**A**) Diphenhydramine hydrochloride, (**B**) lidocaine hydrochloride, (**C**) diazepam, and (**D**) fluoxetine hydrochloride. The top row represents the different modules. Colored modules are active, gray boxes designate inactive modules. Reagent and solvent numbers refer to the compounds listed in table S2.

are included at strategic positions and coupled with data acquisition units to facilitate operational monitoring and support real-time production control. Because few commercial chemically compatible components were available and suitable for the gram-per-hour size scale combined with elevated temperatures and pressures, we developed most of the unit operations used in the upstream and downstream systems, as detailed in the supplementary text. These include pressure sensors, clamshell reactors with an outer aluminum body, and inner PFA (perfluoro alkoxy polymer) tubing for chemical compatibility with good heat transfer (Fig. 1C and fig. S5), surface tension liquid-liquid–driven extraction units (*24*) (Fig. 1C), multiline back pressure regulators (fig. S3), automated precipitation, filtration (Fig. 1D and fig. S6), and crystallization tanks, and automated formulation (Fig. 1D and figs. S7 and S8). The ventilation of this system was designed to have a face velocity between 0.4 and 0.5 m/s, which is typical for chemical fume hoods in the United States.

The units were arranged in modules of reactors and separators to enable reconfiguration to produce the four different drug products within the same system (Fig. 2; see table S2 for the numbering scheme). The synthesis schemes demonstrate the ability to reconfigure the system for increasing levels of chemical complexity, starting with diphenhydramine (Fig. 2A) with one reactor,

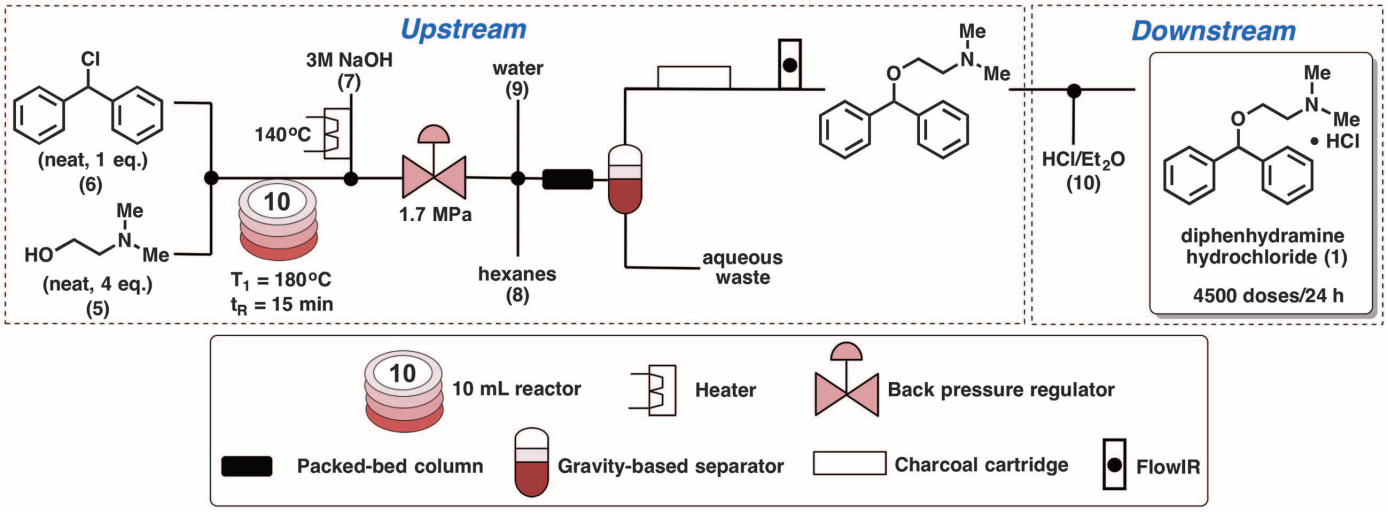

Fig. 3. Synthesis of diphenhydramine hydrochloride using the reconfigurable system. Flowchart detailing the upstream and downstream synthesis.

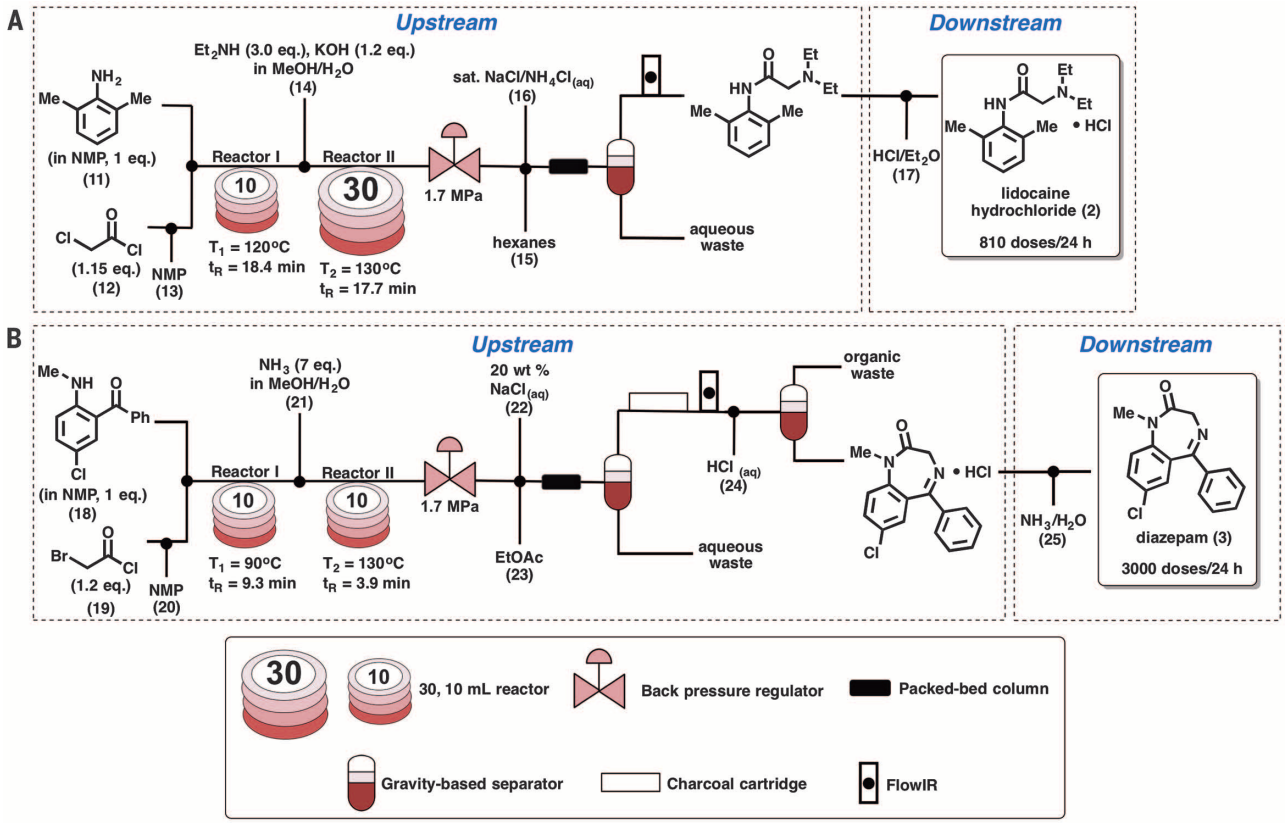

Fig. 4. Synthesis of APIs via two-step upstream configurations. (**A**) Lidocaine hydrochloride and (**B**) diazepam.

one separator, and four pumps and finishing with fluoxetine (Fig. 2D) with four reactors, four separators, and 11 pumps. An inline attenuated total reflection (ATR) Fourier transform infrared (FTIR) system (FlowIR) (figs. S9, S13, S14, S18, and S19) (*25*) provided real-time monitoring of the formed APIs. LabVIEW (National Instruments) programs were also implemented, along with the high- and fast-performance modular X Series data acquisition (DAQ) device and sensors for monitoring multiple process parameters—namely, pressure, reactor temperature, and flow rates. The same LabVIEW platform was also used to automate different units, including heating reactors, pumps, gravity-based separators, and multichannel valves. The downstream module alternatively (Fig. 2, right-hand modules) consisted of precipitation, filtration, redissolution, crystallization, filtration, and formulation units. All drug products were purified and formulated to meet U.S. Pharmacopeia (USP) standards. Consistent with the on-demand format, we focused on concentrated aqueous or alcohol-based formulations ready for dilution to target concentrations when needed and stable for at least 31 days (table S1). Solid formulations, such as tablets, would have required substantial additional space to house unit operations of drying, powder transport, solids blending, and tableting—all processes that would be difficult to implement on the gram-per-hour scale. Nevertheless, we are currently pursuing the miniaturization of these processes so that solid formulations may be prepared on the same platform.

Synthesis and formulation of diphenhydramine hydrochloride

As a first demonstration of the capabilities of this compact unit, diphenhydramine hydrochloride (**1**) was manufactured in its final liquid dosage form. As shown in Fig. 3, the process commenced with the reaction between an excess amount of neat 2-dimethylaminoethanol (**5**) and neat chlorodiphenylmethane (**6**) at a temperature of 180°C and a pressure of 1.7 MPa generated with the use of a back pressure regulator (BPR). The reaction was complete within 15 min, in contrast to typical batch processing requiring 5 or more hours at 125°C in benzene for a similar substrate (*26*). Because the product API has a melting point of 168°C, it could be handled in flow at 180°C in the absence of additional solvent, thereby minimizing the waste generated. The molten salt was then treated with a stream of preheated (140°C) aqueous NaOH (**7**). An inline purification and extraction process employing a packed-bed column to increase mass transfer, a gravity-operated liquid-liquid separator with automatic level control (fig. S1), and an activated charcoal filter to remove the colored impurities produced the diphenhydramine API as a solution in hexanes in 82% yield.

In the downstream section, the API was precipitated with HCl (**10**), and the resulting salt was filtered, washed, and dried in a specially constructed device with a Hastelloy filtration membrane (fig. S6) (*27*). After redissolving in isopropyl alcohol at 60°C, the diphenhydramine hydrochloride (**1**) was recrystallized in a crystallizer, while being cooled to 5°C. Upon filtering and drying, the crystals were dissolved in water. Real-time monitoring using an ultrasonic probe yielded the final dosage concentration (5 ml at 2.5 mg/ml). High-performance liquid chromatography analysis determined that the purity of the product conformed to USP standards (fig. S12) (*28*). Overall, the system capacity based on the optimal yield observed in each step was 4500 doses per day.

The facile transition from **1** to the production of lidocaine hydrochloride (**2**) (Fig. 4; see also Fig. 2B) was next accomplished through simple adjustments of the fluid manifolds to direct the fluids to specific reactors and separators. Whereas **1** was produced via a single upstream reaction, both **2** and **3** were generated through similar two-step upstream configurations, with modifications mainly in the purification and extraction regimens.

Synthesis and formulation of lidocaine hydrochloride

The synthesis of lidocaine hydrochloride (**2**) began with the acylation of 2,6-xylidine (**11**) in *N*-methyl-2-pyrrolidone (NMP) with neat chloroacetyl chloride (**12**), premixed inline with a stream of NMP (**13**) to avoid decomposition on standing (Fig. 4A; see also Fig. 2B). Subsequent addition of a stream of KOH and Et_2NH (**14**) in a mixture of polar protic solvents facilitated the installation of the tertiary amine to generate the crude API, without any intermediate purification. A BPR set at 1.7 MPa after reactor II enabled liquid flow at elevated temperatures (120°C and 130°C), allowing liquid operation well above the boiling point of diethylamine (55°C) and some of the solvents used (methanol and water). As a result, the reaction was complete within 5 min versus batch procedures of 60 min in refluxing toluene (*29*) or 4 to 5 hours in refluxing benzene (*30*). Overall, complete conversion (99%) of the starting materials to the crude API was realized in only 36 min. To deliver the crude lidocaine solution with sufficient purity for a streamlined downstream process, hexane (**15**) and a $NaCl/NH_4Cl$ saturated solution (**16**) were then injected through a cross-junction into the outlet product stream. Upon passing through a packed-bed column containing 0.1-mm glass beads and an inline gravity liquid-liquid separator, lidocaine was obtained in 90% yield. The downstream processing next proceeded with the formation of the HCl salt in a manner similar to that of diphenhydramine. After recrystallization, **2** (88% yield) had a purity of 97.7%, thereby meeting USP standards (fig. S17) (*31*). The API was treated with a premixed aqueous solution of 4% sodium methylcarboxycellulose to yield a final concentrate. Overall, this system can produce 810 doses (dosage strength = 20 mg/ml) of lidocaine hydrochloride per day.

Synthesis and formulation of diazepam

Following the production of lidocaine hydrochloride (**2**), we next transitioned to diazepam (**3**), through switching-in charcoal purification and gravity-based extraction units. As shown in Fig. 4B (see also Fig. 2C), the crude API was synthesized in a two-step upstream sequence initiated with the acylation of 5-chloro-2-(methylamino)

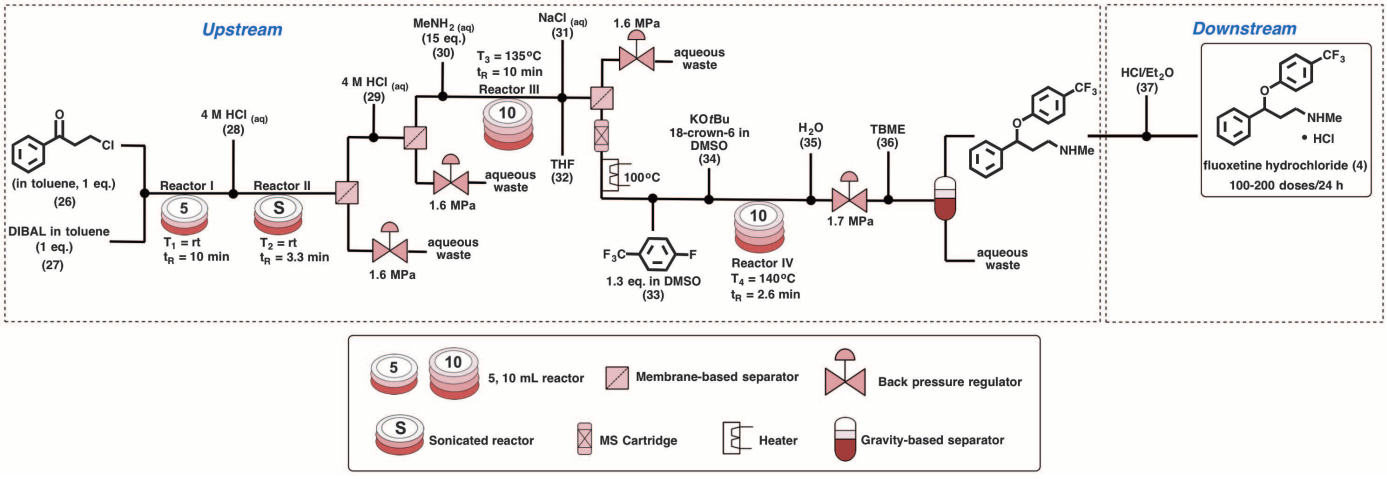

Fig. 5. Demonstration of a multistep API synthesis. Flowchart detailing the upstream and downstream synthesis of fluoxetine hydrochloride. DMSO, dimethyl sulfoxide; rt, room temperature; DIBAL, diisobutylaluminum hydride.

benzophenone in NMP (**18**) with neat bromoacetyl chloride (**19**) premixed inline with a stream of NMP (**20**). Bromine displacement, followed by an intramolecular cyclization reaction upon addition of a stream of NH_3 in MeOH/H_2O (**21**), then furnished the target molecule. Similar to lidocaine, the application of elevated pressure (1.7 MPa) and temperatures (90°C and 130°C) in this sequence enabled liquid flow and complete conversion of the starting materials in only 13 min compared to 24 hours of batch operation at room temperature (*32*). After a continuous extraction, the organic stream was then passed through the activated charcoal cartridge to remove the dark colored dimer and trimer side-products. After precipitation and recrystallization in the downstream section, the dried diazepam crystals (**3**) (94% yield) had a purity level that met USP standards (fig. S22) (*33*). Resuspending in ethanol in the formulation tank then provided a concentrate. At a dosage concentration of 1 mg/ml (one dose is 5 ml at 1 mg/ml), this system can produce ~3000 doses per day.

Synthesis and formulation of fluoxetine hydrochloride

The last of the APIs produced, fluoxetine hydrochloride (**4**), was specifically chosen to demonstrate the versatility and capacity of this system to carry out a complex, fully integrated, telescoped, multistep, biphasic synthesis (Fig. 5; see also Fig. 2D). A series of individual reactions carried out in flow, with purification and isolation of each intermediate in batch, has been previously demonstrated (*34*). By integrating four reactors and four inline separation units, however, we realized the continuous end-to-end synthesis of this API as a racemic mixture. As shown in Fig. 5, the entire upstream reactor network was maintained at 1.7 MPa through the use of multichannel BPR located near the end of the upstream unit. The synthesis commenced with a DIBAL (**27**) reduction of a close-to-saturated solution of 3-chloropropiophenone in toluene (**26**) at room temperature in the first reactor. A stream of 4 M aqueous solution of HCl (**28**) was then introduced, and the resulting mixture was subjected to ultrasound in the second reactor to enable fast dissolution of the aluminum salts and ensure long-term and stable operation of the system (*35*). A two-stage inline extraction and separation sequence with in-house–constructed membrane liquid-liquid/gas separators removed the aqueous waste and gas (*24*). An additional stream of aqueous HCl (**29**) injected into the system before the second separation ensured a complete quench of the reaction.

The intermediate alcohol next reacted with aqueous methylamine (**30**) at 135°C in the third reactor in a biphasic flow. After a residence time of 10 min, tetrahydrofuran (THF) (**32**) and aqueous NaCl (20 mol %) (**31**) efficiently extracted the resulting amino alcohol into a suitable organic solvent (THF) for nucleophilic aromatic substitution in the fourth reactor. Upon separation of the aqueous and organic phase, the latter passed through a cartridge containing 0.4-nm molecular sieves to remove residual water. After a short residence time of 2.6 min in the fourth reactor, the fluoxetine solution merged with a stream of water to prevent the precipitation of the KF salt. Extraction and separation produced a solution of fluoxetine in *tert*-butyl methyl ether (TBME) (**36**) in 43% yield and at a production rate corresponding to 1100 doses per day (one dose is 5 ml at 4 mg/ml) prior to downstream processing. Similar to the other three APIs, the downstream processing involved a precipitation and recrystallization sequence to provide fluoxetine hydrochloride crystals that met USP standards (fig. S25) (*36*). Redissolution in water yielded the final concentrate in 100 to 200 doses.

Overall, the total cycle times for the production and formulation of the APIs varied from 12.2 hours in the case of lidocaine hydrochloride to 47.7 hours for fluoxetine hydrochloride (table S3). Whereas the upsteam syntheses required three residence times (total of 0.7 to 1.3 hours) of the sequential reactions to achieve steady state, the downstream processes took much longer and were mainly dominated by the precipitation step. Because the system featured valves, convenient feed swaps (from reagents to solvents) and fast cleaning procedures between each API production were achieved. Appropriate solvent combinations were added to the reactor lines to flush the up- and downstream units. At the shortest, switching the production of lidocaine hydrochloride to diazepam required a total of 15 min for a complete flush of the internal lines in the upstream section. A switchover from the simplest to the most complex synthesis (diphenhydramine hydrochloride to fluoxetine hydrochloride) would take 2 hours. No cross-contamination was detected from run to run, and the results were reproducible within a standard deviation of 0.6% (diphenhydramine hydrochloride) to 4.7% (fluoxetine hydrochloride) yield for each API production within a single run. The downstream purification and formulation units required no reconfiguration—only the aforementioned flushing. Thus, all transitions between production runs could be completed in less than 4 hours. To meet current good manufacturing practices, one could consider replacing the perfluorinated tubing and membranes in the reactors, BPRs, and separators. The units were designed to facilitate such a replacement.

Outlook

For over a decade, the FDA has been working to stimulate modernization of small-molecule manufacturing, which is largely based on batch manufacturing processes (*37*, *38*). The vision of the FDA's Pharmaceutical Quality for the 21st Century Initiative is to create a more robust and flexible pharmaceutical sector capable of manufacturing high-quality APIs. Continuous manufacturing is one such strategy for meeting this vision (*1*, *39*). Continuous manufacturing systems benefit from integrated processing and control, which can translate to increased safety (no manual handling) and shorter processing times. The use of highly adaptable smaller equipment, which implements real-time monitoring, may also lower production costs and improve product quality (*1*, *37*, *38*). The present implementation of four well-known pharmaceutical drugs demonstrates the concept of continuous, small-scale, on-demand production of pharmaceuticals. Already-demonstrated advances in flow chemistry (*11*–*20*) could be realized on similar platforms, and with additional research, ultimately enable the continuous synthesis of modern small-molecule pharmaceuticals, including enantiopure APIs. The current system focused on liquid oral and topical dosage formulations commensurate with the on-demand approach. A complete alternative platform to current batch manufacturing would inevitably have to produce pharmaceuticals in the common dosage forms of tablets and capsules as well as sterile injectable solutions, which would require advances in downstream processing. Specifically, classical unit operations of crystallization, drying, powder transport, solids blending, and tableting would have to be miniaturized and integrated. New approaches such as three-dimensional printing of tablets could facilitate these developments. Realization and demonstration of good manufacturing practices and ultimately FDA approval will be critical to future applications of this technology, including production units for hospitals, health care organizations, pharmaceutical development, and humanitarian aid.

REFERENCES AND NOTES

1. C. Badman, B. L. Trout, *J. Pharm. Sci.* **104**, 779–780 (2015).
2. I. R. Baxendale *et al*., *J. Pharm. Sci.* **104**, 781–791 (2015).
3. S. Byrn *et al*., *J. Pharm. Sci.* **104**, 792–802 (2015).
4. R. F. Service, *Science* **347**, 1190–1193 (2015).
5. S. Mascia *et al*., *Angew. Chem. Int. Ed.* **52**, 12359–12363 (2013).
6. Food and Drug Administration, *Strategic Plan for Preventing and Mitigating Drug Shortages* (October 2013; www.fda.gov/downloads/Drugs/DrugSafety/DrugShortages/UCM372566.pdf).
7. L. Malet-Sanz, F. Susanne, *J. Med. Chem.* **55**, 4062–4098 (2012).
8. D. Webb, T. F. Jamison, *Chem. Sci.* **1**, 675–680 (2010).
9. R. L. Hartman, J. P. McMullen, K. F. Jensen, *Angew. Chem. Int. Ed.* **50**, 7502–7519 (2011).
10. V. Hessel, *Chem. Eng. Technol.* **32**, 1655–1681 (2009).
11. R. J. Ingham *et al*., *Angew. Chem. Int. Ed.* **54**, 144–148 (2015).
12. B. Gutmann, D. Cantillo, C. O. Kappe, *Angew. Chem. Int. Ed.* **54**, 6688–6728 (2015).
13. M. Baumann, I. R. Baxendale, *Beilstein J. Org. Chem.* **11**, 1194–1219 (2015).
14. F. Lévesque, P. H. Seeberger, *Angew. Chem. Int. Ed.* **51**, 1706–1709 (2012).
15. M. D. Hopkin, I. R. Baxendale, S. V. Ley, *Org. Biomol. Chem.* **11**, 1822–1839 (2013).
16. C. A. Correia, K. Gilmore, D. T. McQuade, P. H. Seeberger, *Angew. Chem. Int. Ed.* **54**, 4945–4948 (2015).
17. M. Viviano, T. N. Glasnov, B. Reichart, G. Tekautz, C. O. Kappe, *Org. Process Res. Dev.* **15**, 858–870 (2011).
18. P. Zhang, M. G. Russell, T. F. Jamison, *Org. Process Res. Dev.* **18**, 1567–1570 (2014).
19. D. Ghislieri, K. Gilmore, P. H. Seeberger, *Angew. Chem. Int. Ed.* **54**, 678–682 (2015).
20. P. R. D. Murray *et al*., *Org. Process Res. Dev.* **17**, 1192–1208 (2013).
21. P. L. Heider *et al*., *Org. Process Res. Dev.* **18**, 402–409 (2014).
22. Materials and methods are available as supplementary materials on *Science* Online.
23. D. J. am Ende, in *Chemical Engineering in the Pharmaceutical Industry*, D. J. am Ende, Ed. (Wiley, NJ, 2011), chap. 1.
24. A. Adamo, P. L. Heider, N. Weeranoppanant, K. F. Jensen, *Ind. Eng. Chem. Res.* **52**, 10802–10808 (2013).
25. C. F. Carter *et al*., *Org. Process Res. Dev.* **14**, 393–404 (2010).
26. G. Rieveschl, Dialkylaminoalkyl benzhydryl ethers and salts thereof, U.S. Patent 2,421,714A, 3 June 1947.

27. S. Y. Wong, J. Chen, L. E. Forte, A. S. Myerson, *Org. Process Res. Dev.* **17**, 684–692 (2013).
28. USP (U.S. Pharmacopeia), *Monograph* **34**, 2597 (2014).
29. T. J. Reilly, *J. Chem. Educ.* **76**, 1557 (1999).
30. N. M. Loefgren, B. J. Lundqvist, Alkyl glycinanilides, U.S. Patent 2,441,498, 11 May 1948.
31. USP (U.S. Pharmacopeia), *Monograph* **37**, 3552–3553 (2014).
32. T. Sugasawa, M. Adachi, T. Toyoda, K. Sasakura, *J. Heterocycl. Chem.* **16**, 445–448 (1979).
33. USP (U.S. Pharmacopeia), *Monograph* **37**, 2580–2581 (2014).
34. B. Ahmed-Omer, A. J. Sanderson, *Org. Biomol. Chem.* **9**, 3854–3862 (2011).
35. R. L. Hartman, J. R. Naber, N. Zaborenko, S. L. Buchwald, K. F. Jensen, *Org. Process Res. Dev.* **14**, 1347–1357 (2010).
36. USP (U.S. Pharmacopeia), *Monograph* **37**, 3035–3036 (2014).
37. Food and Drug Administration, *FDA Perspective on Continuous Manufacturing*, (February 2013; www.fda.gov/downloads/AboutFDA/CentersOffices/OfficeofMedicalProductsandTobacco/CDER/UCM341197.pdf).
38. S. L. Lee *et al.*, *J. Pharm. Innov.* **10**, 191–199 (2015).
39. S. D. Schaber *et al.*, *Ind. Eng. Chem. Res.* **50**, 10083–10092 (2011).

ACKNOWLEDGMENTS

Authors are listed in alphabetical order. We thank A. Clayton for elements of the system design, S. H. Harrison for the LabVIEW programming downstream, and A. T. Carlson for assistance with the design of the downstream units. We also thank L. M. Heckman and J. M. Noss for assistance with development of chemistry. This work was supported by the Defense Advanced Research Project Agency (DARPA) and Space and Naval Warfare Systems Center Pacific (SSC Pacific) under Contract no. N66001-I I-C-4147. We thank E. Choi, D. T. McQuade, J. Lewin, and G. Ling for their advice and support. The data reported in this paper are available in the article or in the supplementary materials. A.A. is founder of Zaiput Flow Technologies. T.F.J. is a cofounder of Snapdragon Chemistry, Inc., and a scientific adviser for Zaiput Flow Technologies, Continuus Pharmaceuticals, Paraza Pharmaceuticals, and Asymchem. K.F.J. is a scientific adviser for Snapdragon Chemistry, Inc. A.S.M. is a scientific adviser to GenSyn Technologies, Blues Spark Technologies, Continuus Pharmaceuticals, and Goddard Laboratories. MIT has filed a patent on behalf of A.A., M.B., T.F.J., K.F.J., J.C., A.S.M., J.-C.M.M., E.M.R., D.R.S., T.S., N.W., S.Y.W., and P.Z.

SUPPLEMENTARY MATERIALS

www.sciencemag.org/content/352/6281/61/suppl/DC1
Materials and Methods
Figs. S1 to S25
Tables S1 to S3
References (*40*–*43*)

21 December 2015; accepted 22 February 2016
10.1126/science.aaf1337

REPORTS

STELLAR EVOLUTION

A white dwarf with an oxygen atmosphere

S. O. Kepler,[1]* Detlev Koester,[2] Gustavo Ourique[1]

Stars born with masses below around 10 solar masses end their lives as white dwarf stars. Their atmospheres are dominated by the lightest elements because gravitational diffusion brings the lightest element to the surface. We report the discovery of a white dwarf with an atmosphere completely dominated by oxygen, SDSS J124043.01+671034.68. After oxygen, the next most abundant elements in its atmosphere are neon and magnesium, but these are lower by a factor of ≥25 by number. The fact that no hydrogen or helium are observed is surprising. Oxygen, neon, and magnesium are the products of carbon burning, which occurs in stars at the high-mass end of pre–white dwarf formation. This star, a possible oxygen-neon white dwarf, will provide a rare observational test of the evolutionary paths toward white dwarfs.

White dwarf stars are the end product of stellar evolution for all stars born with masses below 8 to 11 solar masses ($M_\odot$). The limit depends on the initial composition on the main sequence, in particular the abundances of the heavy elements (the metallicity), but also on uncertainties of the models and input physics. Among these are the nuclear reaction rates of C+He and C+C and the treatment of convection in the asymptotic giant branch (*1*, *2*). About 80% of white dwarfs have atmospheres dominated by H, and the remainder by He. All other elements are only small traces, much less abundant than in the Sun. The reason for this unusual pattern is separation in the strong gravitational field (*3*). The lightest elements present very rapidly float to the surface once the white dwarf cools below about 100,000 K effective temperature ($T_{\rm eff}$). Except for the basic division of the two groups, which suggests different evolutionary channels, the atmosphere of the white dwarfs in their later cooling evolution has thus lost all memory of the previous evolutionary phases. There are only a few, very rare, exceptions to this rule. At very high effective temperature, $T_{\rm eff}$ > 200,000 K, two stars (H1504+65 and RX J0439.8-6809) (*4*) show no visible He or H but a C/O mixture. The limits on the He abundance are rather high, and it is quite possible that these stars will develop H or He atmospheres as they cool to lower effective temperatures, when gravitational separation becomes efficient.

Between 22,000 K ≥ $T_{\rm eff}$ ≥ 18,000 K, there is a small group of stars, called Hot DQ white dwarfs (*5*, *6*), which have C-dominated atmospheres. Their origin is not yet clear, but a likely scenario is that the carbon is dredged up from below the atmosphere once the convection zone reaches deep enough (*7*). If this scenario is correct, the DQ stars demonstrate that underneath the He layer there is a C layer resulting from the previous He-burning stage on the asymptotic giant branch. Another scenario is their formation by a merger of two white dwarf stars (*8*). At lower effective temperature, around 12,000 K, there is another small group of stars with strong O lines in their spectra; they have He-dominated atmospheres, but the next most abundant element is O, followed by C (*9*–*11*). It is plausible that their composition is related to the pre–white dwarf evolution, specifically C burning, but the reason that they appear at this temperature and this O/C ratio is not understood. To aid in our understanding of the late phases of low and intermediate mass star evolution, we searched for new white dwarf stars through the 4.5 million spectra in Data Release (DR) 12 (*12*) of the Sloan Digital Sky Survey (SDSS) (*13*).

One of the results of our search was SDSS J124043.01+671034.68 (spectrum with Plate-Modified Julian Date-Fiber 7120-56720-0894), which covers 3600 to 10,400 Å with resolving power $R = \lambda/\delta\lambda \sim 2000$. The spectrum (Fig. 1) exhibits many O I spectral lines, appearing similar to the group of cool stars with strong oxygen lines in their spectra (*10*, *11*). The absence of any He lines could be understood if the stellar effective temperature were near 11,000 K. However, closer inspection shows several lines of ionized Mg II and even O II, which require $T_{\rm eff}$ > 20,000 K. Temperatures ~20,000 K are also obtained from the SDSS photometry and the ultraviolet Galaxy Evolution Explorer (GALEX) measurements (*14*). At this temperature, the H and He lines, if these elements were present in the atmosphere, should be very strong. The absence of any He and H lines is only possible if O is the most abundant element. A detailed analysis (see the supplementary materials) confirmed this, with $T_{\rm eff}$ = 21,600 K and surface gravity $\log g = 7.93 \pm 0.17$, where $g = GM/R^2$ is the surface gravity in centimeter-gram-second units, with G the gravitational constant, M the stellar mass, and R the radius. Table 1 shows the atmospheric composition ratios determined from our modeling (see the supplementary materials).

The surface gravity is typical for white dwarfs (*13*) and corresponds to a mass of $0.56 \pm 0.09\ M_\odot$, using the white dwarf mass-radius relation for stars without outer H layer (*15*), but it is theoretically not expected for a star with an oxygen atmosphere. From the estimated $\log g$ solution and the SDSS photometry in the *ugriz* filters,

[1]Instituto de Física, Universidade Federal do Rio Grande do Sul, 91501-900 Porto Alegre, RS, Brazil. [2]Institut für Theoretische Physik und Astrophysik, Universität Kiel, 24098 Kiel, Germany.
*Corresponding author. E-mail: kepler@if.ufrgs.br

www.sciencemag.org/content/352/6281/61/suppl/DC1

Supplementary Materials for

On-demand continuous-flow production of pharmaceuticals in a compact, reconfigurable system

Andrea Adamo, Rachel L. Beingessner, Mohsen Behnam, Jie Chen, Timothy F. Jamison,* Klavs F. Jensen,* Jean-Christophe M. Monbaliu, Allan S. Myerson,* Eve Revalor, David R. Snead, Torsten Stelzer, Nopphon Weeranoppanant, Shin Yee Wong, Ping Zhang

*Corresponding author. E-mail: tfj@mit.edu (T.F.J); kfjensen@mit.edu (K.F.J); myerson@mit.edu (A.S.M)

Published 1 April 2016, *Science* **352**, 61 (2016)
DOI: 10.1126/science.aaf1337

This PDF file includes:

Materials and Methods

Drug Products

For reference purposes, commercial samples of fluoxetine hydrochloride (**4**) and lidocaine hydrochloride (**2**) were purchased from Shunyi Bio-Chemical Technology Co, Ltd, China. Diazepam (**3**) and diphenhydramine hydrochloride (**1**) were purchased from Sigma Aldrich, USA and Alfa Aesar, USA, respectively. All other chemicals were purchased from Sigma-Aldrich, and used as received, unless otherwise noted. Deionized (DI) water was obtained from a Milli-Q, Millipore system. Samples were treated under process conditions on the bench prior to off-line analysis. NMR analysis was performed on a Varian Mercury 300 MHz or Varian Inova-500 MHz spectrometer in the specified deuterated solvent. The ^{1}H NMR data is reported as follows: chemical shift in parts per million (ppm), multiplicity (s = singlet, d = doublet, t = triplet, q = quartet, m = multiplet), coupling constant in hertz (Hz) and integration.

In-line IR Monitoring

In-line, real-time reaction monitoring was carried out with a FlowIR from Mettler-Toledo with a DTGS Detector using HappGenzel apodization, equipped with a SiComp (Silicon) probe connected via a FlowIR sensor. Sampling was performed from 4000 to 650 cm^{-1} at 8 wavenumber resolution with 208 scans. In-line monitoring was implemented for diphenhydramine, lidocaine and diazepam. Examples of IR libraries for these APIs are illustrated in figures S9, S13, S18, S19 as well as an example of an in-line IR process monitoring for lidocaine in fig. S14.

In-line Ultrasound Monitoring

In-line, real-time formulation monitoring was carried out with a LiquiSonic 30 from SensoTech GmbH, Germany, equipped with a Hastelloy probe measuring temperature and ultrasonic velocity (*40*). Examples of standard curves for diphenhydramine hydrochloride, lidocaine hydrochloride, diazepam, and fluoxetine hydrochloride are illustrated in figures S10, S15, S20, S23.

Upstream Units

Automated gravity-based separator. The automated gravity-based liquid-liquid separator (fig. S1) consisted of a Dean-Stark tube and a capacitive sensor (FirstSensor, USA) that monitored the interface between the organic and aqueous streams. By controlling the aqueous stream outlet, complete separation between the aqueous and organic streams was achieved.

Membrane-based separators. The membrane-based liquid-liquid separator used in the syntheses was designed to be chemically compatible by machining the wetted parts in perfluorinated polymers (ETFE for the internal structure, PTFE for the porous membrane and PFA for the impermeable diaphragm of the pressure controller) (*24*, *41*). It was also designed to have high-pressure ratings by encapsulating the perfluorinated components in a metal shell. Aluminum performed well for sustaining the mechanical stress generated by pressurized fluids and provided strong threads for the fittings. FEP coated o-rings provided a leak proof device up to about 2.0 MPa of pressure and bolts completed the

assembly (fig. S2). The separator was designed for a maximum flow rate of about 10 mL/min.

Back pressure regulators (BPRs). Dome loaded-type BPRs (*42*) were designed in which the liquid flow path is intercepted by a diaphragm, loaded, on the other side, by a compressed gas (fig. S3, top) that sets the value of the back pressure. A diaphragm with a low mass and modest thickness (125 µm) was selected so that the pressure of the compressed gas would be practically identical to the cracking point of the BPR. This design was proven to ensure accuracy and operational flexibility since any value of back pressure between 0 and 2.0 MPa was achievable without the need for changing the device or without stepwise increments of the set point, as it would be with preset devices. Since the chamber with compressed air used to set the back pressure value can be sealed, the operation of the regulator can be independent of the availability of a compressed gas. Alternatively, by keeping the regulator connected to an adjustable compressed gas source, changes to the BPR set point can be achieved dynamically during operation. The selection of perfluorinated materials for the wetted parts (EFTE for the main internal body and PFA for the diaphragm) provided the required wide chemical compatibility. An aluminum shell completed the outer body of the BPR. The same concept was extended for the design of the multiple inlet BPR, suitable for applications that would require the exact same pressure set point for several reactor lines. A modified version (fig. S3, bottom) combining a common compressed gas chamber with 4 ports was successively used for the complex process scheme of fluoxetine. Testing of the BPR (fig. S4) with water showed the set point was within 1% across values ranging from 0 to 2 MPa and flow rates ranging from 0.1 to 100 mL min^{-1}.

Reactors. Continuous-flow tubular reactors of defined volumes (5, 10, 30 mL) were made with coils of extreme-purity PFA tubing (1/8" O.D., McMaster-Carr) wrapped around an aluminum cylinder and embedded in aluminum shells. PFA coils provide chemical resistance, but the combination of heat and pressure renders PFA typically unsuitable for use. However, the addition of an aluminum shell provides a way to extend the use of the tubing to higher temperature and pressure values since the metal takes the mechanical load. Additionally, heaters (Omega Engineering, CT - USA) were embedded in the central aluminum cylinder to facilitate the heat transfer to the PFA coil. The high heat conduction coefficient of aluminum and the aspect ratio with sides of the block of comparable length ensured a uniform temperature distribution in the metal. A thermocouple was inserted in each reactor for monitoring and temperature control (Omega Engineering, CT – USA). The heat conduction to the fluids occurs through the tubing wall and the temperature profile can be analytically calculated with standard theory (Graetz problem with constant wall temperature) (*43*). A 10 mL tubular reactor is depicted in fig. S5.

Downstream Units

Filtration-drying-dissolution unit (FDD). The FDD mounted in a 45° angle operates by distributing the slurry on top of a sintered 0.5 graded Hastelloy plate (Mott Corporation) while vacuum is applied through the porous plate (fig. S6) (*27*). The downstream vacuum is enabled through transfer lines to the waste tank connected to a

vacuum pump (UN811 KVP, KNF Neuberger). Once the residual mother liquor is removed, the vacuum is closed by a solenoid valve (Type 0127, Christian Bürkert GmbH & Co. KG) and wash solvent is pumped into the FDD and pulled through the porous plate by opening the valve after washing. The solenoid valves with PEEK (polyether ether ketone) manifolds and FFPM (perfluoro-polymer) sealing material are utilized for all subunits downstream. The subsequent vacuum drying step is initiated by heating the FDD with a wrapped flexible heater (KH series, Omega Engineering, Inc) controlled by a T-type thermocouple (TJC36 series, Omega Engineering, Inc). Once the drying step is complete, the valve is closed and solvent is pumped into the FDD to re-suspend the dried solids to be transferred to the subsequent unit by opening the in-house built bottom drain valve (BDV).

Commercial BDVs suitable for slurry transportations were well outside the space capabilities of this current platform. Thus BDVs were built in-house and utilized for all subunits downstream, which take advantage of gravity as the driving force for the slurry transportation. BDVs open and close using a plunger driven by a servo motor (pulse width modulation (PWM) controlled). The outlets of the subunits and BDVs have a diameter of 10 mm to prevent clogging issues.

Holding and formulation tank. The holding and formulation tank is a 500 mL HDPE vessel equipped with an ultrasound sensor (LiquiSonic30, SensoTech GmbH) and PTFE coated marine impeller (fig. S7). Here, the concentration and temperature is monitored and adjusted as necessary by solvent addition and a thermoelectric liquid cooler (LC-035, TE Technology, Inc.) respectively, before the solution is pumped into the subsequent unit by opening the valve.

Crystallizer. The crystallizer is a 120 mL jacketed HDPE vessel equipped with a PTFE coated marine impeller (fig. S8). The temperature is controlled with a thermoelectric liquid cooler (LC-200, TE Technology, Inc.) to provide sufficient cooling capacity to ensure cooling rates below room temperature.

Synthesis Protocols.

Synthesis of diphenhydramine hydrochloride (**1**).

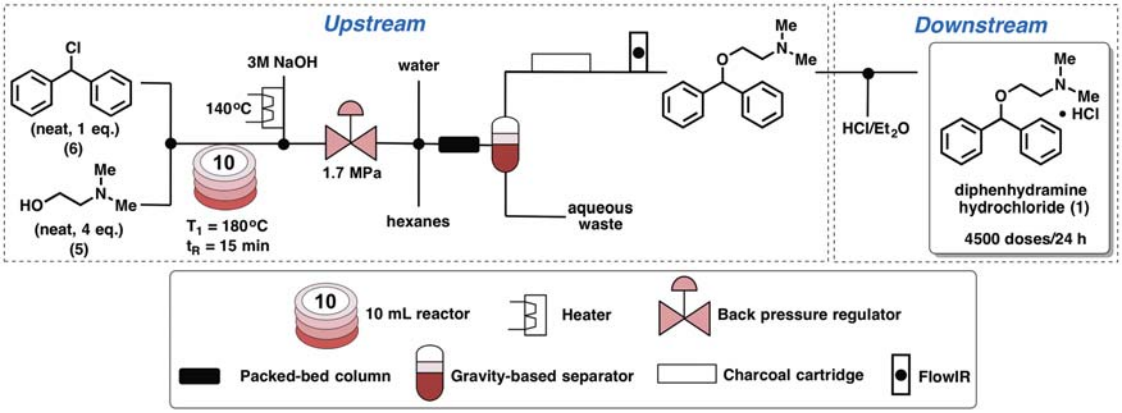

Upstream processing. Chlorodiphenylmethane (**6**) (neat, 1 equivalent) (flow rate 0.2 mL/min) and an excess amount of 2-dimethylaminoethanol (**5**) (neat, 4 equivalents) (flow rate 0.46 mL/min) were combined in a 10 mL reactor at 180 °C and a pressure of 1.7

MPa. After a residence time of 15 min, a stream of preheated 3 M aqueous sodium hydroxide (140 °C) (flow rate 2.7 mL/min) was injected to quench the HCl. The crude diphenhydramine was then extracted by concomitant injection of a mixture of hexanes and DI water at a flow rate of 2.7 mL/min. After flowing through a short packed-bed column of 0.1 mm glass beads, the organic phase was separated from the aqueous waste via a gravity-operated liquid-liquid separator. Filtration through activated charcoal provided a 0.36 M solution of diphenhydramine (**1**) (82% yield) in hexane. Real-time qualitative monitoring of this process was accomplished using an in-line attenuated total reflection (ATR) Fourier Transform InfraRed (FTIR) system (FlowIR) (fig. S9).

Downstream processing. The crude solution was pumped into a buffer tank. Upon reaching the desired minimum volume (300 mL), it was transferred into the precipitation tank cooled at 10 °C and equipped with a propeller impeller while stirring at 200 rpm. A solution of 0.5 M hydrochloric acid in diethyl ether was then added at a rate of 0.5 mL/min while stirring at 200 rpm until a 1:1 molar ratio was obtained. After 1 h, the precipitated salt was filtered using a specially constructed filter/dryer unit made of high density polyethylene (HDPE) featuring a Hastelloy filtration membrane. The material was subsequently washed with 100 mL of cold hexane and dried in the same unit under vacuum at room temperature for 1 h. The dried salt was then dissolved in isopropanol (196.5 mg/mL) at 60 °C and crystallized in a 100 mL HDPE crystallizer equipped with a propeller type impeller, while being cooled 1 °C /minute to a final temperature of 5 °C. After filtering the slurry and drying the crystals in a combined filter dryer unit at 70 °C, they were dissolved in DI water. Real-time monitoring of the ultrasonic velocity of the solution using an ultrasonic probe (LiquiSonic 30, SensoTech GmbH) enabled the final dosage concentration of 2.5 mg/mL (see fig. S10 for the standard curve). The purity of the diphenhydramine salt was measured using HPLC (106%) and conformed to the USP standards (*28*).

See fig. S11 for the NMR spectra.

^{1}H NMR of the free base (300 MHz, $CDCl_3$) δ: 7.43-7.13 (m, 10H), 5.38 (s, 1H), 3.59 (t, J = 6.0 Hz, 2H), 2.62 (t, J = 6.0 Hz, 2H), 2.28 (s, 6H)

^{13}C NMR of the free base (75 MHz, $CDCl_3$) δ: 142.5, 128.6, 127.6, 127.2, 84.3, 67.8, 59.2, 46.3

Characterization by HPLC. HPLC analysis of diphenhydramine hydrochloride (**1**) was performed by injecting 10 µL onto an Agilent 1260 Infinity system equipped with an Agilent Zorbax SB-CN column (4.6x250 mm, 5µm packing) maintained at 25 °C and a UV detector (254 nm). The mobile phase was pumped at a constant flow rate of 1 mL/min and consisted of a mixture of water, acetonitrile and triethylamine (50:50:0.5, V/V) adjusted with glacial acetic acid to a pH of 6.5. The characteristic retention time of diphenhydramine hydrochloride (**1**) is 6-8 min (fig. S12).

Synthesis of lidocaine hydrochloride (**2**).

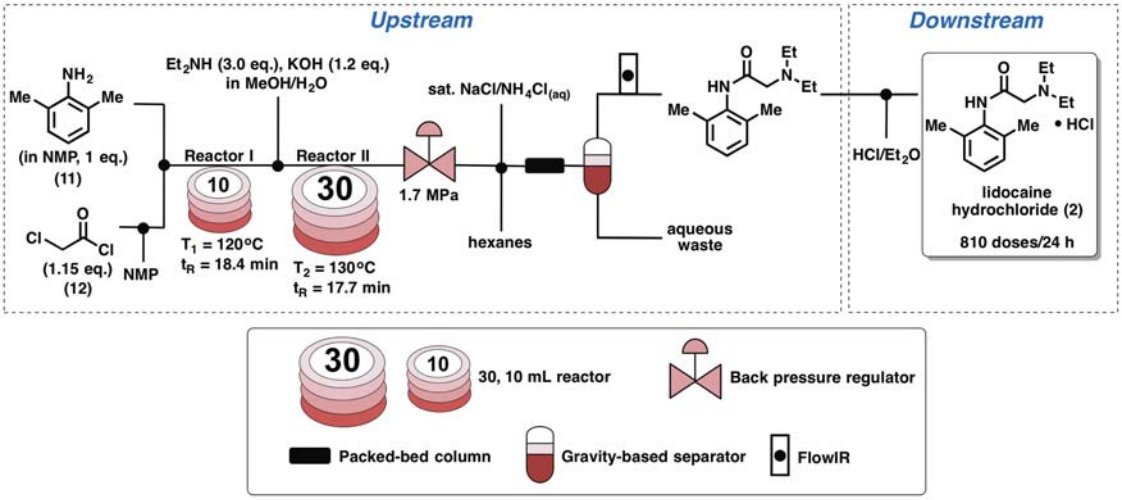

Upstream processing. Streams of neat chloroacetyl chloride (**12**) (1.15 equivalents) (flow rate 2.7 mL/h), *N*-methyl-2-pyrrolidinone (NMP) (0.15 mL/min) and a 1.43 M solution of 2,6-xylidine (**11**) (1.0 equivalents) in NMP (0.35 mL/min) were combined in a 10 mL reactor (Reactor I) at 120 °C. After a residence time of 18.4 min, KOH (1.2 equivalents) and diethylamine (3.0 equivalents) in a 1:1 solution of MeOH and DI water (1.15 mL/min) was introduced and the mixture was maintained in Reactor II at 130 °C for 17.7 min. A back pressure regulator set at 1.7 MPa was used after the second coil reactor. HPLC analysis revealed complete conversion (99%) of 2,6-xylidine (**11**) to the crude lidocaine. The outcoming stream of the API (flow rate 1.65 mg/mL, 0.15 M) was then extracted by concomitant injection of hexane (3 mL/min) and a saturated solution of NaCl and NH_4Cl (2 mL/min). After flowing through a short packed-bed column of 0.1 mm glass beads, the organic phase was separated from the aqueous waste via a gravity-operated liquid-liquid separator and monitored in real-time in-line via FlowIR (fig. S13, S14). Steady state was reached after 60 minutes and lidocaine was obtained in 90% yield as a solution in hexane.

Downstream processing. Once 250 mL of this crude 0.11 M solution was pumped (3 mL/min) into the buffer tank, it was then transferred into the precipitation tank. A solution of hydrochloric acid in diethyl ether (82.5 mL, 0.5 M) was then added at a flow rate of 0.2 mL/min. The molar ratio of the acid solution to the crude API was 1.5:1. The precipitation was performed at 10 °C and once complete, the slurry was filtered and the crystals were washed with 250 mL hexane and dried under vacuum at 50 °C for 1 h. The salt was subsequently recrystallized by an antisolvent cooling crystallization process in a 100 mL HDPE crystallizer equipped with a propeller type impeller rotating at 200 rpm. Specifically, the recrystallization was performed by conveying 60 mL of a solution of acetone and isopropanol (96/4 wt%) into the crystallizer. Hexane was then added as the antisolvent (40 vol%, flow rate 2 mL/min). The contents were cooled from 50 °C to 5 °C at a rate of 1 °C /min and then held at 5 °C for 2 h. Using this procedure the API was obtained in 88% yield and with a purity of 97.7%, thereby meeting USP standards (*31*). After filtration, the crystals were washed with 100 mL of hexane and dried under vacuum at 50 °C for 2 h. A premixed mixture (50 mL) consisting of 4% sodium methylcarboxy

cellulose in DI water was then added to the crystals while stirring at 200 rpm. The solution was drained into the formulation tank and the concentration of the concentrate (34.9 mg/mL) was determined using an ultrasonic probe (LiquiSonic 30, SensoTech GmbH) (see fig. S15 for the standard curve).

See fig. S16 for the NMR spectra.

^{1}H NMR of the free base (300 MHz, $CDCl_3$) δ: 8.93 (brs, 1H), 7.11-7.06 (m, 3H), 3.22 (s, 2H), 2.69 (q, J = 7.0 Hz, 4H), 2.22 (s, 6H), 1.13 (t, J = 7.5 Hz, 6H)

^{13}C NMR of the free base (75 MHz, $CDCl_3$) δ: 170.4, 135.2, 134.1, 128.4, 127.2, 57.6, 49.1, 18.8, 12.8

Characterization by HPLC. HPLC analysis of lidocaine hydrochloride (**2**) was performed by injecting 20 µL onto an Agilent 1260 Infinity system equipped with an Agilent Pursuit 5 C18 column (3.9x300 mm) maintained at 25 °C and a UV detector (254 nm). The mobile phase was pumped at a constant flow rate of 1.5 mL/min and consisted of a 1:4 (V/V) mixture of acetonitrile and Solution A (water and glacial acetic acid, 930:50, V/V) adjusted with 1M sodium hydroxide to a pH of 3.4. The characteristic retention time of lidocaine hydrochloride (**2**) is 4-6 min (fig. S17).

Synthesis of diazepam (**3**).

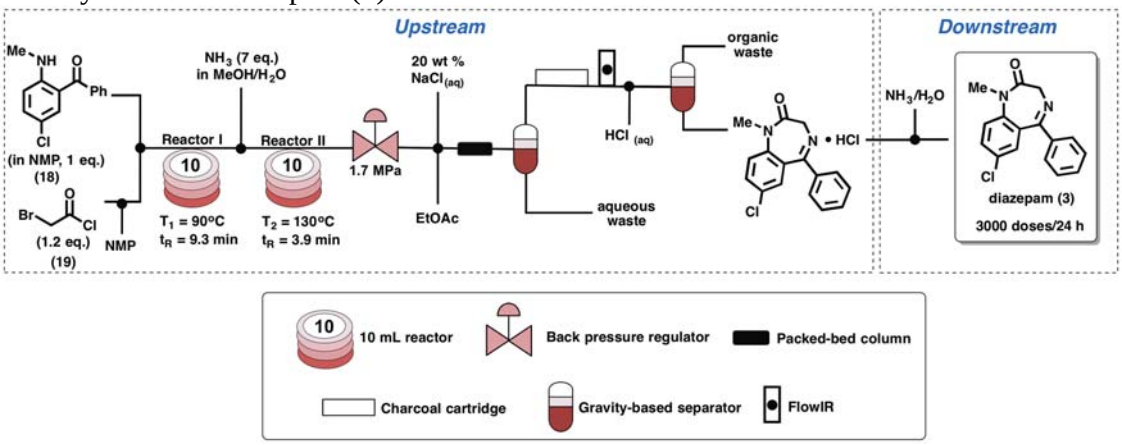

Upstream processing. Neat bromoacetyl chloride (**19**) (1.2 equivalents) (flow rate 4.4 mL/h) was diluted with NMP (0.25 mL/min) and then combined with a 1 M solution of 5-chloro-2-(methylamino)benzophenone (**18**) (1.0 equivalents) in NMP (flow rate 0.75 mL/min) in a 10 mL reactor (Reactor I). After 9.3 min at 90 °C, a solution of NH_3 (7 equivalents) in methanol and DI water (9:1) was added and the mixture was maintained in Reactor II for a residence time of 3.9 min at 130 °C. A back pressure regulator positioned after Reactor II ensured a pressure of 1.7 MPa. HPLC analysis revealed a 95% conversion of the starting materials and a 78% yield of the target API. The crude mixture contained several side products including the starting benzophenone, intermediate halides and their hydrolysis adducts as well as dimers/trimers and cyclohexenone derivatives. The crude diazepam was then extracted by concomitant injection of EtOAc (flow rate 5 mL/min) and a 20 wt% aqueous solution of sodium chloride (flow rate 2.5 mL/min).

After passing through a short packed-bed column containing 0.1 mm glass beads and a gravity-operated liquid-liquid separator, the resulting organic stream was transferred through a cartridge loaded with activated charcoal to remove the dark colored by-products (e.g. dimers and trimers). Real-time monitoring of this process was achieved using an in-line silicon IR probe (fig. S18-S19). A continuous acid wash (4 M HCl) to remove the non-basic organic impurities, followed by a separation, provided a 0.1 M solution of the crude diazepam salt.

Downstream Processing. The crude solution was pumped into a buffer tank. Upon reaching the desired minimum volume (250 mL), it was transferred into the precipitation tank equipped with a propeller impeller while stirring at 320 rpm. Precipitation of the API was induced at 10 °C by the addition of a 28% ammonium hydroxide solution in DI water (93 mL) at a flow rate of 0.3 mL/min. The slurry was then filtered and the resulting filter cake was washed with 250 mL of DI water and dried under vacuum at 50 °C for 1 h. The material was subsequently recrystallized in a 100 mL HDPE crystallizer equipped with a propeller type impeller rotating at 200 rpm. For the crystallization process, DI water (70 vol%) was used as the antisolvent and was added at a flow rate of 2 mL/min to a solution of diazepam in DMSO (initial concentration of 21.6 mg/mL). After a holding time of 2 h at 25 °C, the API was obtained in 94% yield and with a purity of 104.3%, thereby meeting USP standards (*33*). The slurry was then drained and the crystals were washed with 100 mL of DI water while filtering. The filter cake was dried under vacuum at 60 °C for 4 h and resuspended and dissolved in 40 mL of EtOH while stirring at a rate of 200 rpm. After the solution was drained into the formulation tank, the concentration of the concentrate (7.8 mg/mL) was determined using an ultrasound probe (LiquiSonic 30, SensoTech GmbH) (see fig. S20 for the standard curve).

See fig. S21 for the NMR spectra.

^{1}H NMR of the free base (300 MHz, $CDCl_3$) δ: 7.63-7.55 (m, 2H), 7.54-7.36 (m, 4H), 7.33-7.23 (m, 2H), 4.83 (d, J = 12.0 Hz, 1H), 3.77 (d, J = 12.0 Hz, 1H), 3.39 (s, 3H)

^{13}C NMR of the free base (75 MHz, $CDCl_3$) δ: 170.3, 169.3, 142.9, 138.5, 131.8, 131.0, 130.4, 130.2, 129.8, 129.6, 128.7, 122.8, 57.3, 35.2

Characterization by HPLC. HPLC analysis of diazepam (**3**) was performed by injecting 10 µL onto an Agilent 1100 system equipped with an Agilent Pursuit 5 C18 column (3.9x150 mm) maintained at 25 °C and a UV detector (254 nm). The mobile phase was pumped at a constant flow rate of 1 mL/min and consisted of a 2:2:1 (V/V) mixture of water, acetonitrile and methanol. The characteristic retention time of diazepam (**3**) is 3-5 min (fig. S22).

Synthesis of fluoxetine hydrochloride (**4**).

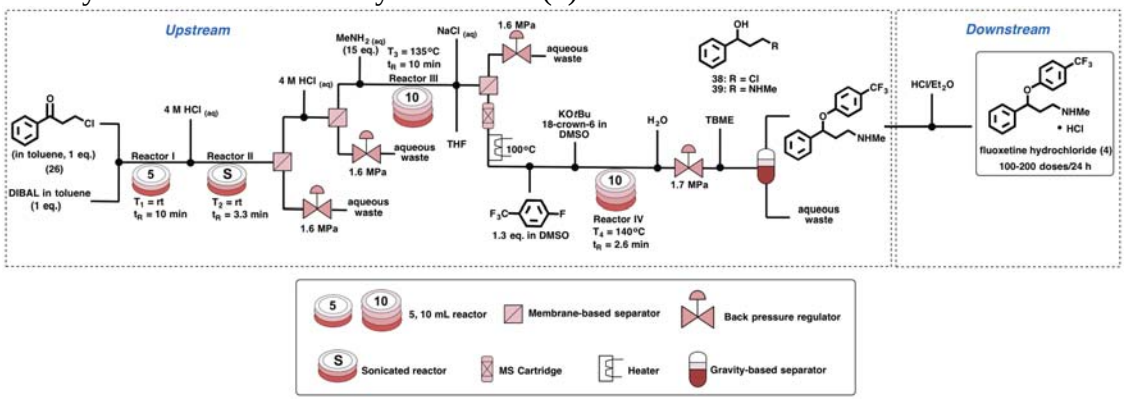

Upstream processing. 3-Chloropropiophenone (**26**) (3 M in toluene) (flow rate 0.12 mL/min) was treated with a 1 M solution of DIBAL in toluene at a flow rate of 0.36 mL/min at room temperature in a 5 mL spiral reactor (Reactor I). The reaction reached completion after 10 minutes on a 0.36 mmol min^{-1} scale (96% yield). After the addition of an aqueous solution of 4 M HCl, (flow rate 1 mL/min) the material was passed into an ultrasonic transducer (Reactor II) to ensure fast dissolution of the aluminum salts. A two-stage in-line extraction and separation sequence was then implemented with successive membrane liquid-liquid separators to remove the aqueous waste and gas from the DIBAL decomposition (91% yield post-separation). A second stream of aqueous 4 M HCl (flow rate 1 mL/min) was injected into the system prior to the second separation to completely quench the reaction. The intermediate alcohol **38** (0.75 M in the main toluene stream) was then directed to a 10 mL spiral reactor (Reactor III) for a biphasic amination reaction with aqueous methylamine (40% wt in DI water, flow rate 0.5 mL/min) under slug-flow conditions. The conversion of the starting alcohol reached 93% after a residence time of 10 minutes at 135 °C (89% yield). The crude amino alcohol **39** was then efficiently extracted (90% after in-line separation) by concomitant injection of THF (0.5 mL/min) and an aqueous solution of 20 wt% sodium chloride (flow rate 2 mL/min). After the organic phase was separated, it was passed through a cartridge loaded with molecular sieves (MS, 4Å) to remove the residual DI water. The amino alcohol **39** was then preheated and treated with consecutive streams of 4-fluorobenzotrifluoride in DMSO (0.24 M) at a flow rate of 1.7 mL/min and potassium *tert*-butoxide (0.25 M)/18-crown-6 (0.05 M) in DMSO at a flow rate of 1.29 mL/min. After a residence time of 2.6 min (Reactor IV), a stream of DI water was injected to avoid precipitation of the KF salt and clogging of the back pressure regulator. Injection of TBME followed by a gravity-operated liquid-liquid separation, provided the crude fluoxetine as a solution (43% overall yield).

Downstream Processing. The crude solution of fluoxetine (7.5 mg/mL) in TBME was then pumped (flow rate 4.6 mL/min) into the buffer tank. Upon reaching the desired minimum volume (300 mL) the solution was transferred into a precipitation tank pre-loaded with 50 mg of (**4**) seed crystals and equipped with a propeller impeller stirring at 320 rpm. A 2 M HCl/diethyl ether (10 mL) solution was added at a flow rate of 0.5 mL/min. Hexane was then added as an antisolvent (60 mL) at a flow rate of 0.5 mL/min. The resulting slurry was ripened for 36 h at 3 °C and the precipitated salt was filtered

using a specially constructed filter/dryer unit made of HDPE featuring a Hastelloy filtration membrane. After washing with 250 mL of hexane, the filter cake was dried under vacuum at 50 °C for 1 h. The crude salt was then dissolved in acetone at 50 °C and recrystallized in a two-stage antisolvent cooling crystallization process. In the first stage, 50 mL of the solution was conveyed into the 100 mL HDPE crystallizer equipped with a propeller type impeller while rotating at 120 rpm. The antisolvent hexane (37.5 vol%) was added while the mixture was cooled from 50 °C to 5 °C at a rate of 1 °C /min. The mixture was then held at 5 °C for 2 h. The resulting slurry was filtered and dried in a combined filter dryer unit at 60 °C for 1 h. The filter cake was dissolved again in acetone at 50 °C, recrystallized in a second crystallizer (stage two) and filtered as described above for the first crystallization process. The concentration of fluoxetine hydrochloride in acetone was 26.3 mg/mL in stage one and 21.2 mg/mL in stage two. The average yield of both stages was 74% and a purity (HPLC) of 93.0% and 102.0% was obtained, respectively. The material after the second recrystallization stage conformed to USP standards (*36*). The crystals obtained after drying the slurry from stage two were then dissolved in DI water and the concentration of the concentrate (5.2 mg/mL) was determined using an ultrasonic probe (LiquiSonic 30, SensoTech GmbH) (see fig. S23 for the standard curve).

See fig. S24 for the NMR spectra.

^{1}H NMR of the free base (500 MHz, $CDCl_3$) δ: 7.44 (d, J = 10.0 Hz, 2H), 7.36-7.26 (m, 5H), 6.92 (d, J = 10.0 Hz, 2H), 5.33 (dd, J = 10.0, 5.0 Hz, 1H), 2.79-2.75 (m, 2H), 2.45 (s, 3H), 2.26-2.18 (m, 1H), 2.07-2.00 (m, 1H), 1.81 (brs, 1H)

^{19}F NMR of the free base (282 MHz, $CDCl_3$, ref $CF_3C_6H_5$) δ: -62.4

Characterization by HPLC. HPLC was performed by injecting 10 µL of fluoxetine hydrochloride onto an Agilent 1100 instrument equipped with a UV diode array detector (227 nm). The column used was a Phenomenex Luna C8(2) 250 mm x 4.60 mm ID, packed with 5 µm base-deactivated particles, pore size 100 Å and temperature controlled at 25 °C. The mobile phase consisted of a 6:3:1 (V/V) ratio of triethylamine buffer (10 mL of triethylamine in 980 mL of water, adjusted to a pH value of 6 with phosphoric acid), tetrahydrofuran (stabilizer-free) and methanol. The mobile phase was pumped at a constant flow rate of 1 mL/min. The characteristic retention time of fluoxetine hydrochloride (**4**) is 12-14 min (fig. S25).

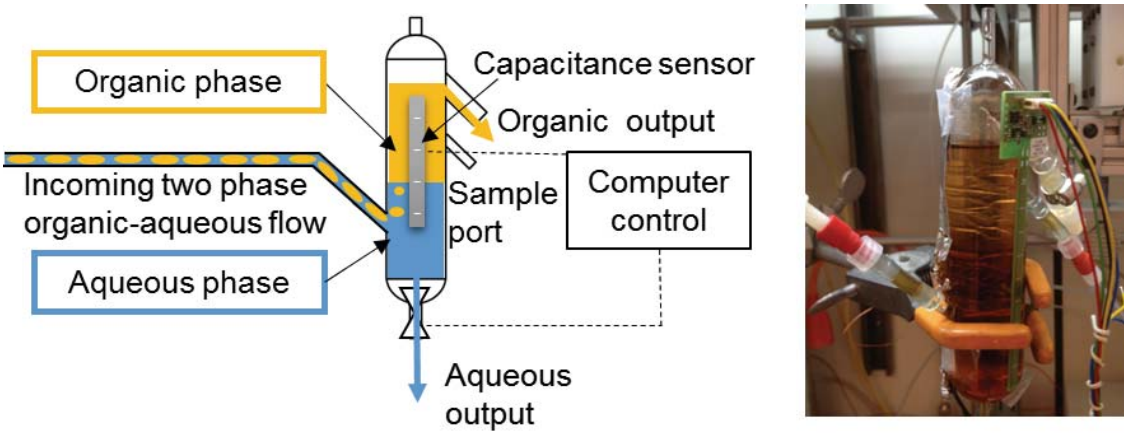

Fig. S1. Automated gravity-based separator. Left schematic, right photograph.

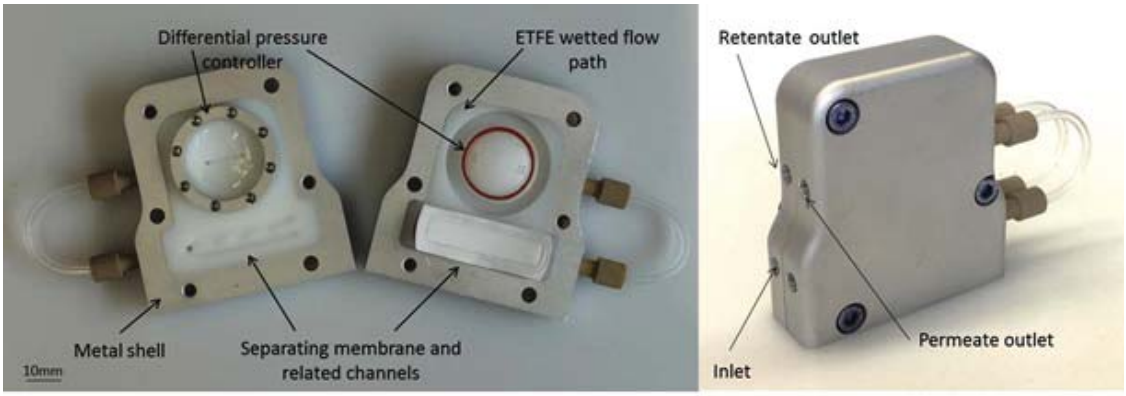

Fig. S2. Liquid-liquid separator. The left image is an opened separator whereas the right image shows an assembled separator ready for use.

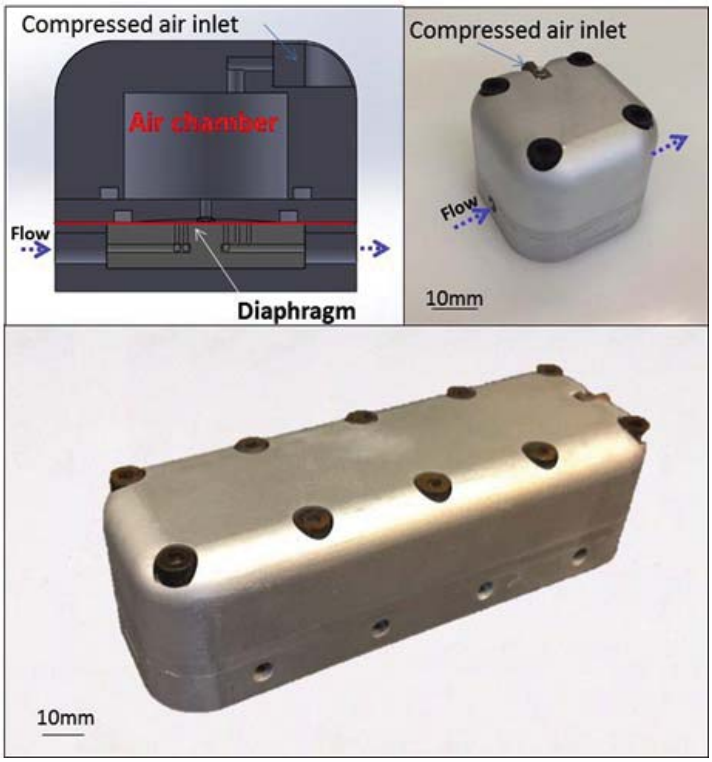

Fig. S3. Back pressure regulator. (Top left) Cross section of the device with the flow path and diaphragm identified. (Top right) Assembled single device. (Bottom) In the four port device, the common pressurized air chamber assures equal set points across the 4 different channels.

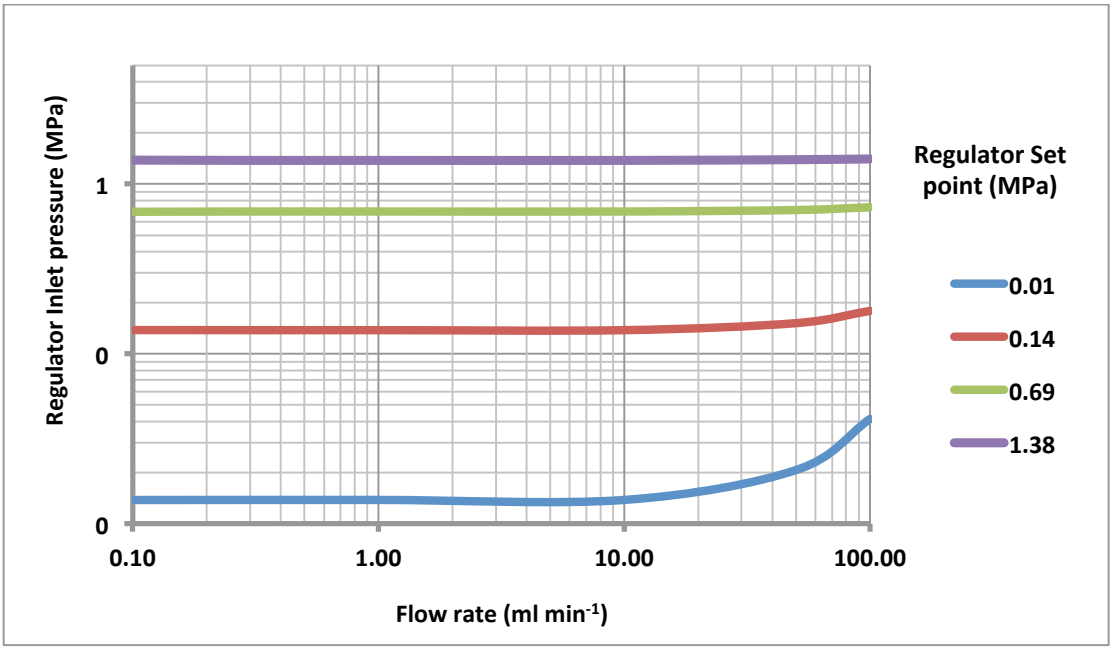

Fig. S4. Back pressure regulator (BPR) performance with liquids (water). In the x-axis, flow rates; in the y-axis, pressure measured at the inlet of the BPR; the parameter is the set point of the BPR. The BPR exhibits high accuracy across a wide range of flow rates and set points, although some deviation is observed for high flow rates (> 10 mL min^{-1}) and a very low set point (0.01 MPa).

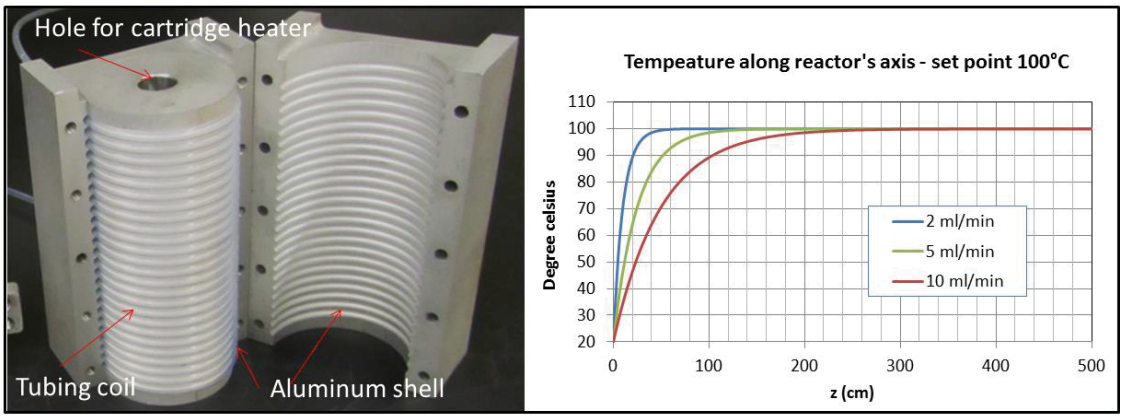

Fig. S5. Reactor (10 mL). (Left) The PFA tubing coil (1/8’’OD-1/16’’ ID) can be recognized. The shell has an adequate shape to fully encapsulate and constrain the tubing to provide a pressure rating. A hole on the top houses a cartridge heater. (Right) Theoretical temperature distribution along the tube in a 10 mL reactor for a stream entering at 20 °C, set temperature of 100 °C and flow rates of 2, 5 and 10 mL min^{-1}.

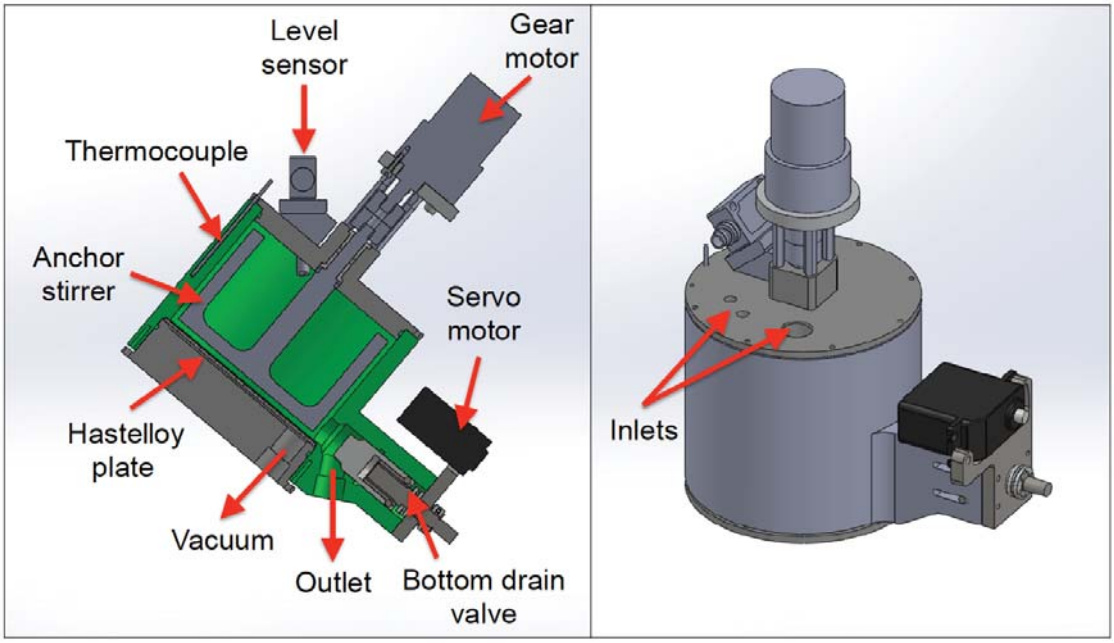

Fig. S6. Filtration-drying-dissolution unit (FDD) equipped with bottom drain valve, thermocouple, porous Hastelloy plate, PTFE coated anchor stirrer, level sensor, and overhead motor. The left image shows the cross-section while the right shows the 3D model.

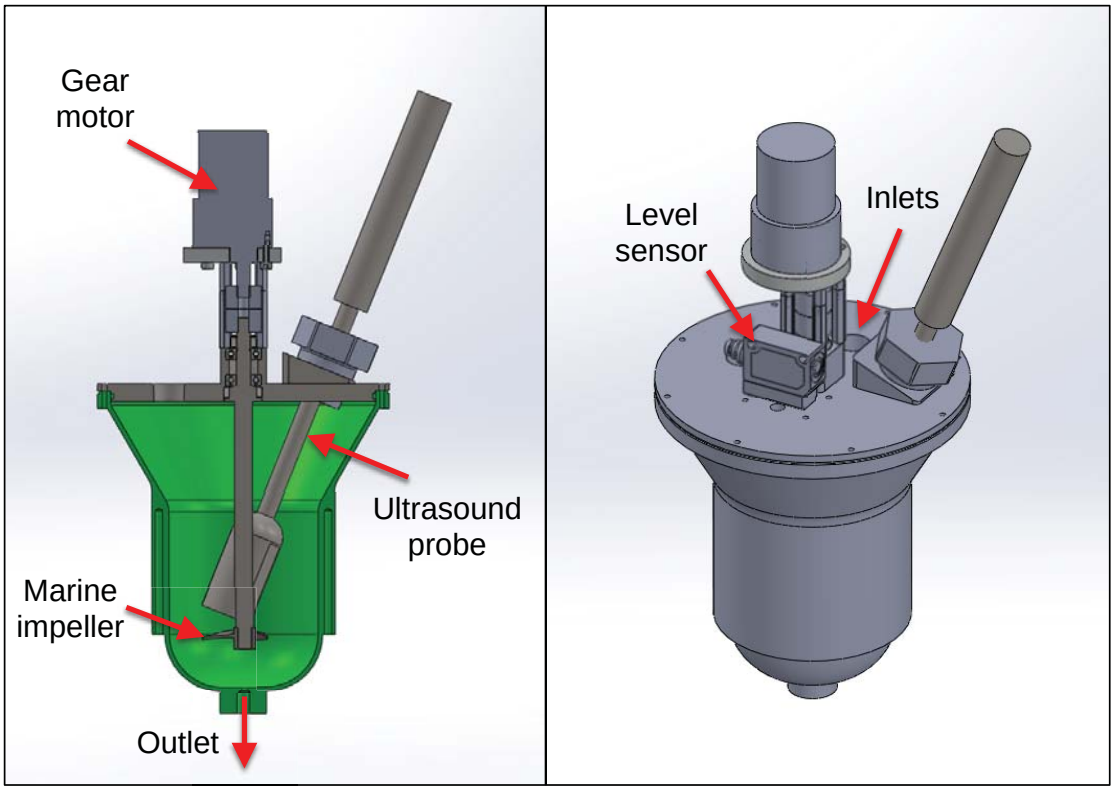

Fig. S7. Holding tank equipped with ultrasound probe, PTFE coated marine impeller, level sensor, and overhead motor. Left shows the cross-section whereas the right shows the 3D model.

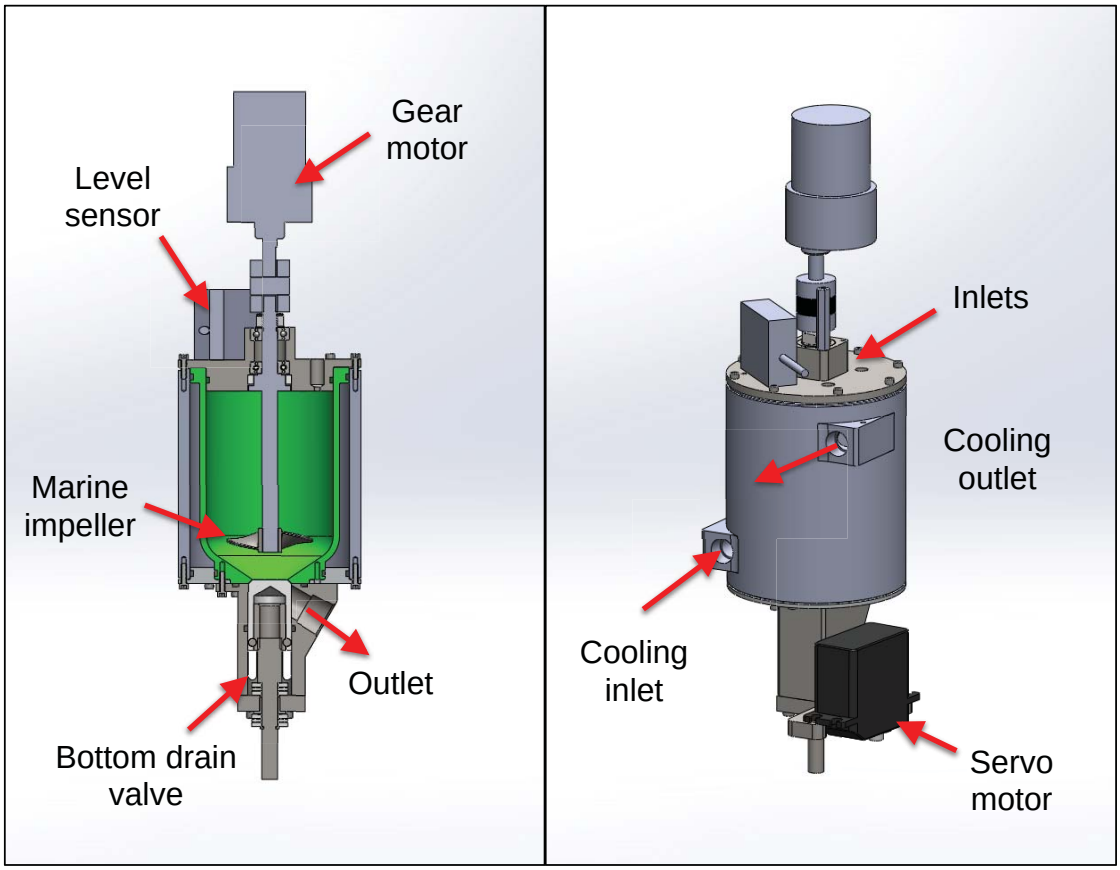

Fig. S8. Crystallizer equipped with bottom drain valve, PTFE coated marine impeller, and level sensor. Left shows the cross-section whereas the right shows the 3D model.

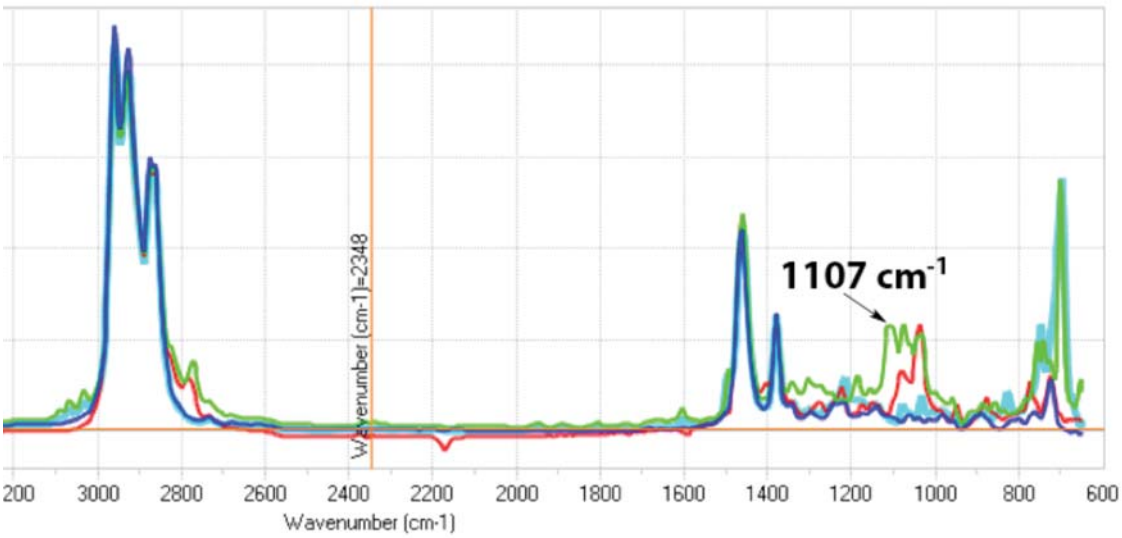

Fig. S9. IR spectral library for diphenhydramine. Solutions of diphenhydramine (green), 2-dimethylaminoethanol (red) and chlorodiphenylmethane (light blue) in hexanes (dark blue) were utilized as standards for the IR library. The characteristic peak at 1107 cm^{-1} was used to monitor the reaction.

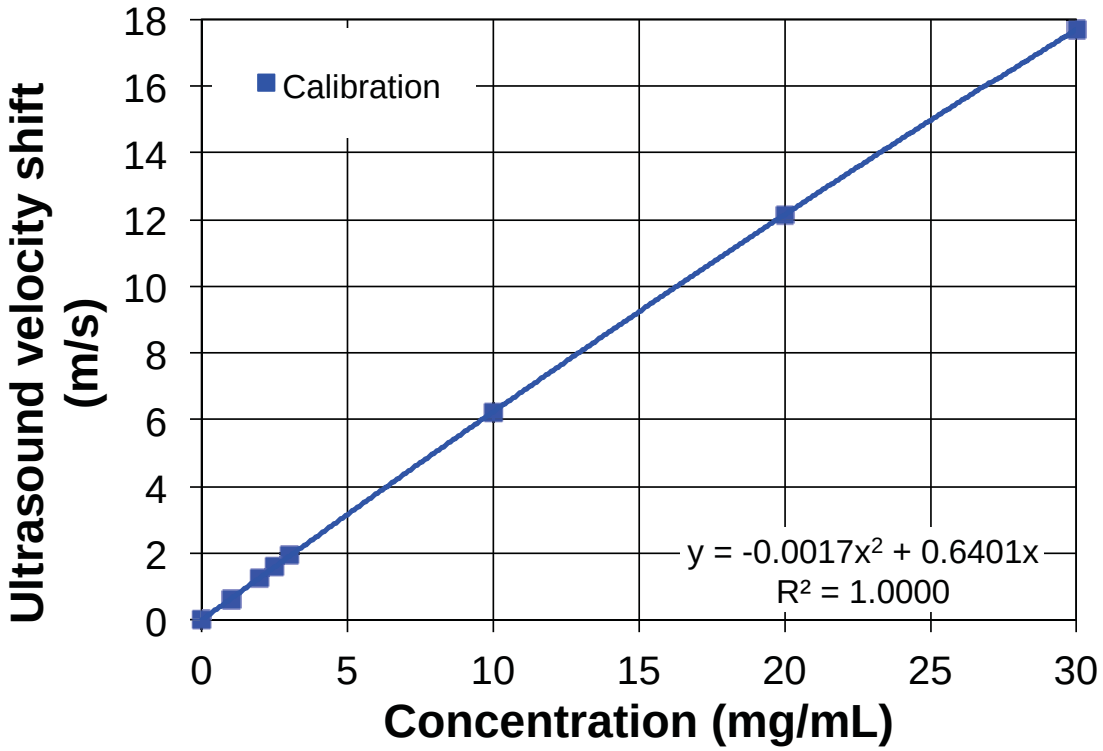

Fig. S10. Standard curve of the ultrasonic velocity as a function of diphenhydramine hydrochloride concentration in water. This curve was used to determine the concentration of diphenhydramine hydrochloride (**1**) in the formulation tank.

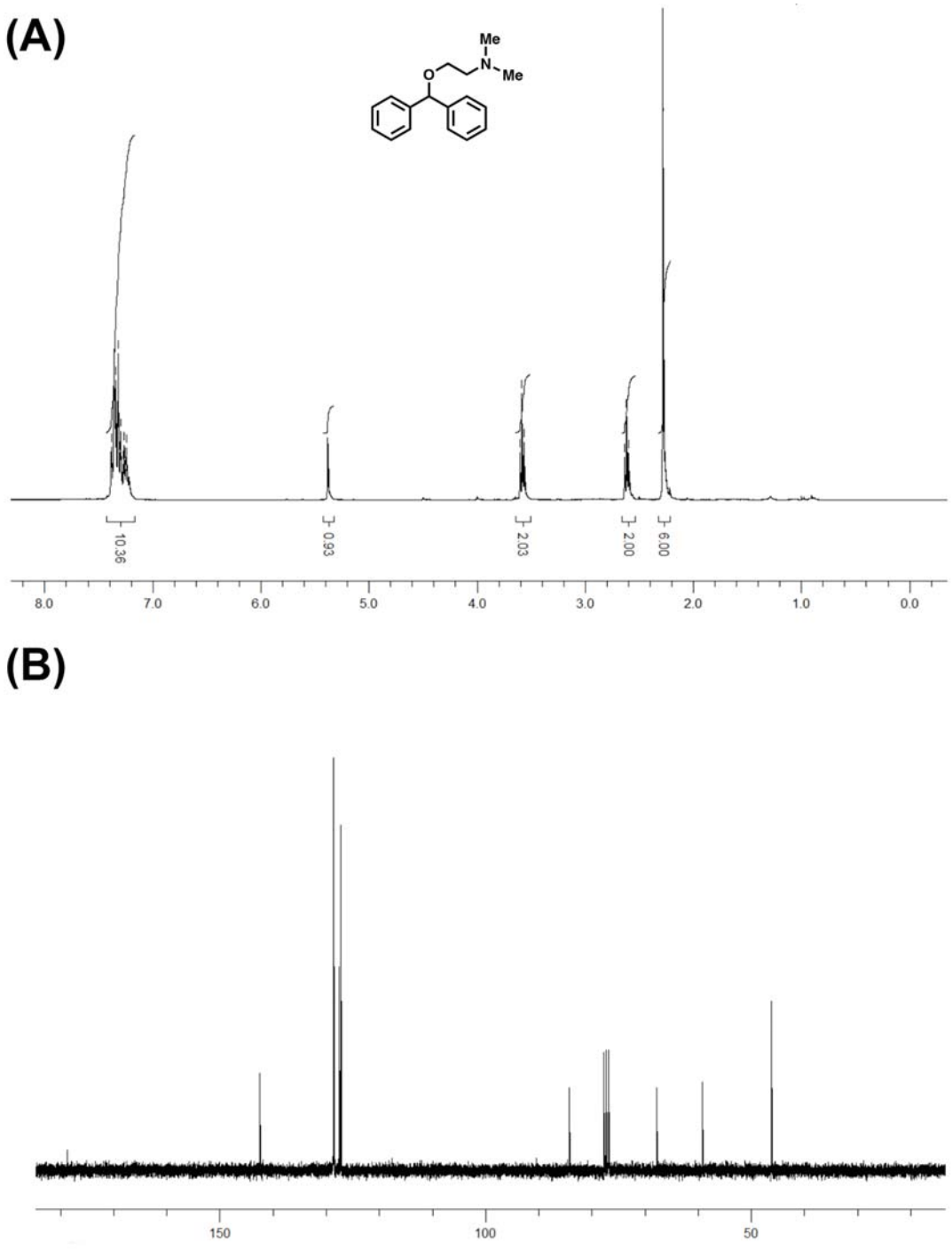

Fig. S11. (A) ^{1}H NMR (300 MHz, $CDCl_3$) and (B) ^{13}C NMR (75 MHz, $CDCl_3$) spectra of crude diphenhydramine obtained from the upstream unit after evaporating the hexanes.

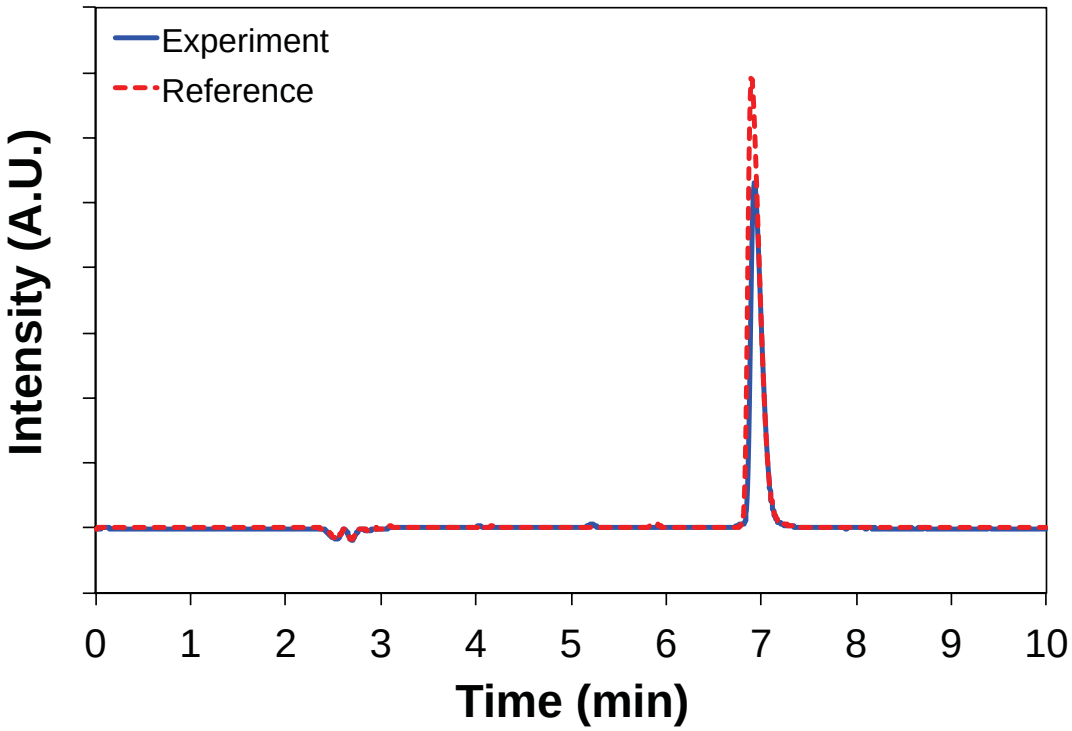

Fig. S12. Chromatogram of diphenhydramine hydrochloride (**1**) produced using the system (solid blue line) compared to the commercial reference (dashed red line).

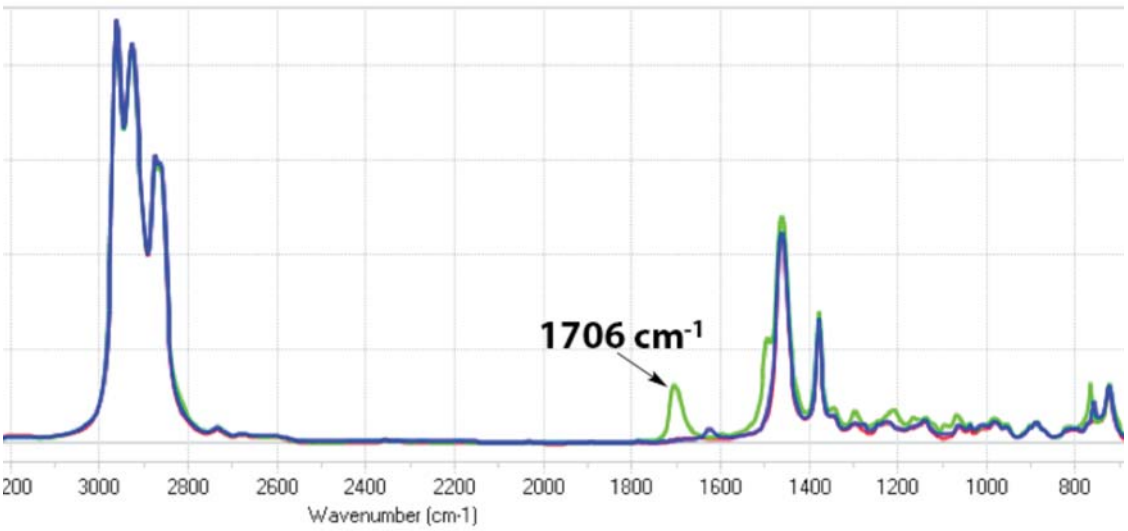

Fig. S13. IR spectral library for lidocaine in hexanes. Solutions of 2,6-xylidine (dark blue), and lidocaine (green) in hexanes (red) were utilized as standards for the IR library. The characteristic peak at 1706 cm^{-1} for lidocaine (ν_{CO}) was used to monitor the reaction.

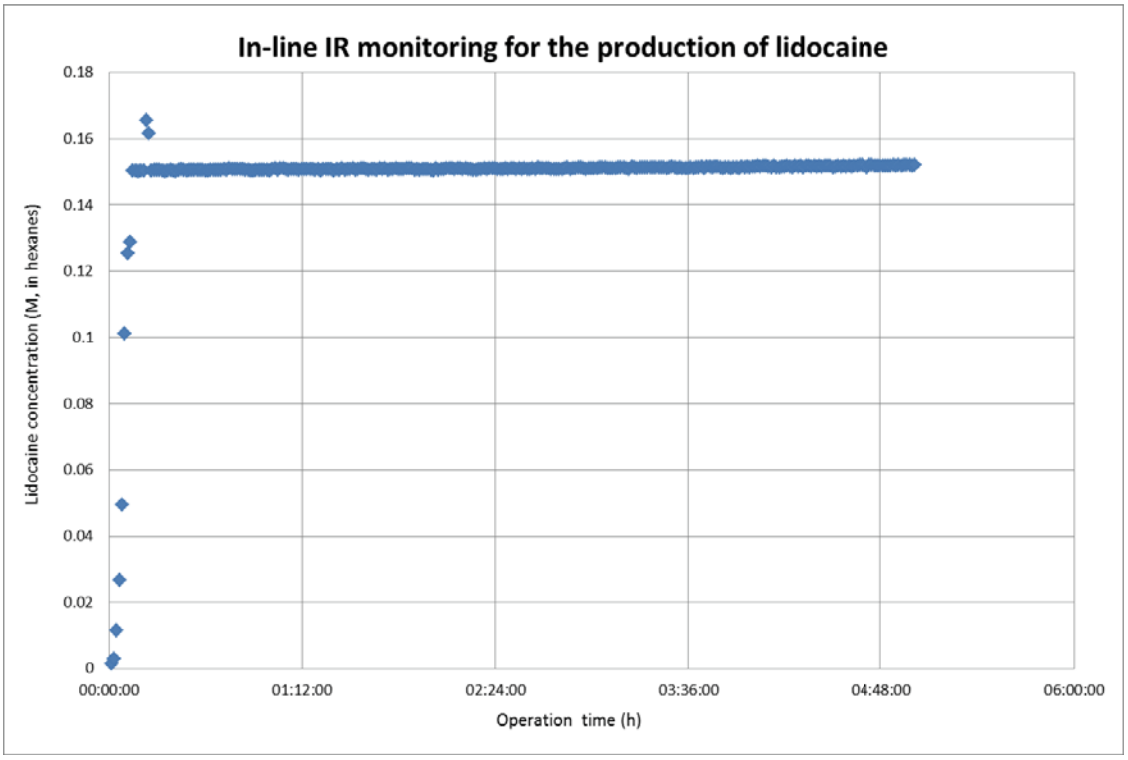

Figure S14. In-line, real-time continuous monitoring of the production of lidocaine. Calibration of the Flow IR was performed with standardized solutions of lidocaine in hexanes using the ICQant software. The production of lidocaine was monitored over 5 hours of operation at steady state. After 6 hours of operation, some lidocaine began to accumulate on the surface of the silicon sensor. The IR cell was flushed with acetone to eliminate the residue.

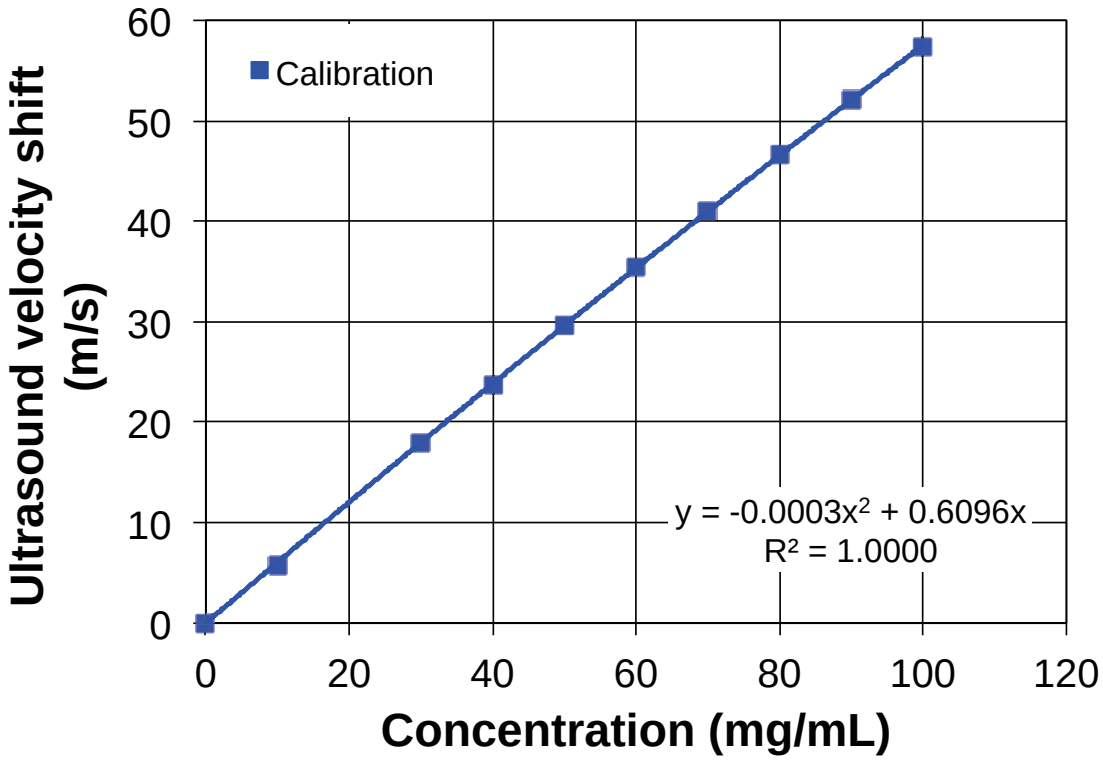

Fig. S15. Standard curve of the ultrasonic velocity as a function of lidocaine hydrochloride concentration in an aqueous solution of 4% sodium methylcarboxycellulose. This curve was used to determine the concentration of lidocaine hydrochloride (**2**) in the formulation tank.

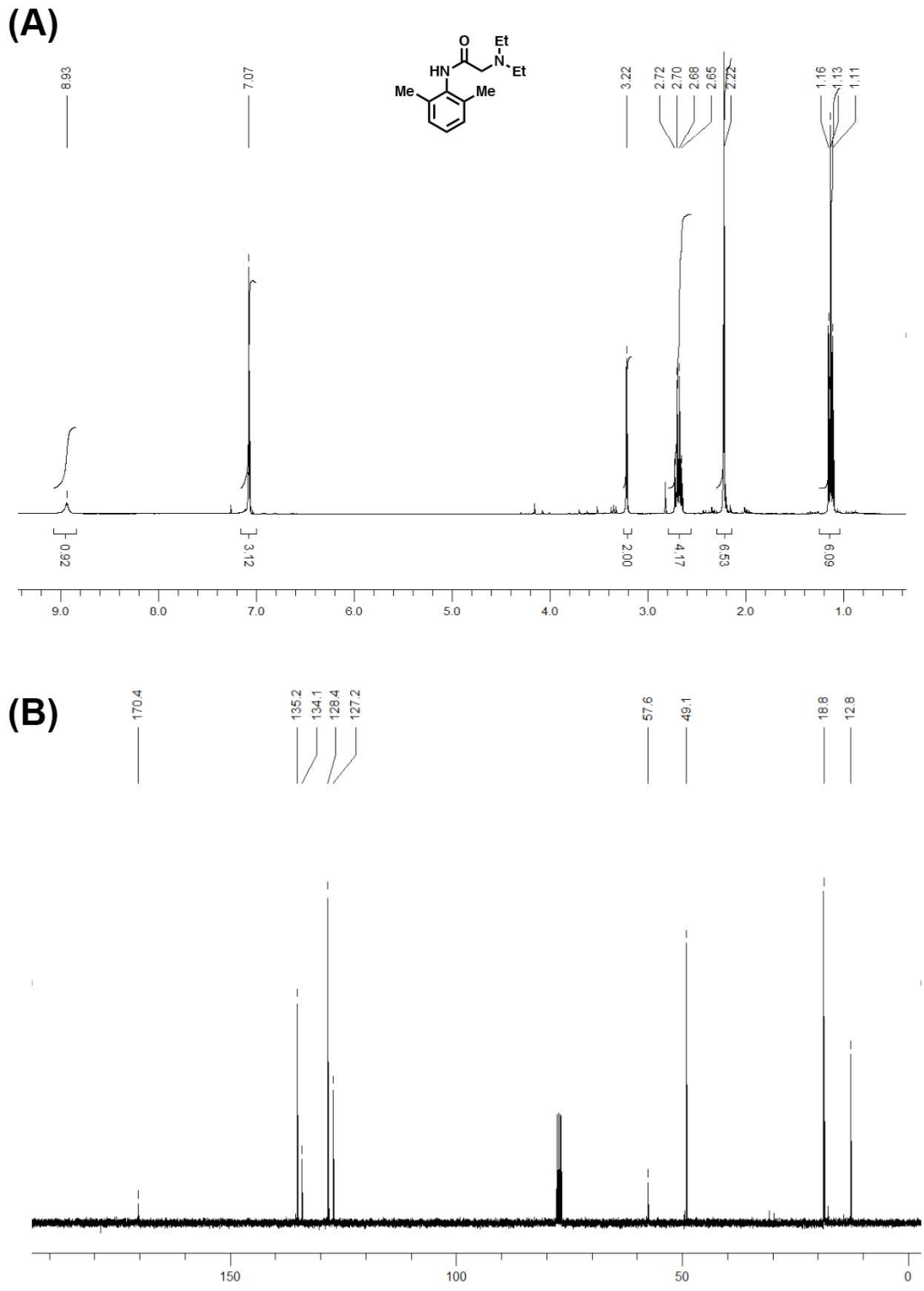

Fig. S16. (A) ^{1}H NMR (300 MHz, $CDCl_3$) and (B) ^{13}C NMR (75 MHz, $CDCl_3$) spectra of crude lidocaine obtained from the upstream unit after evaporating the hexanes.

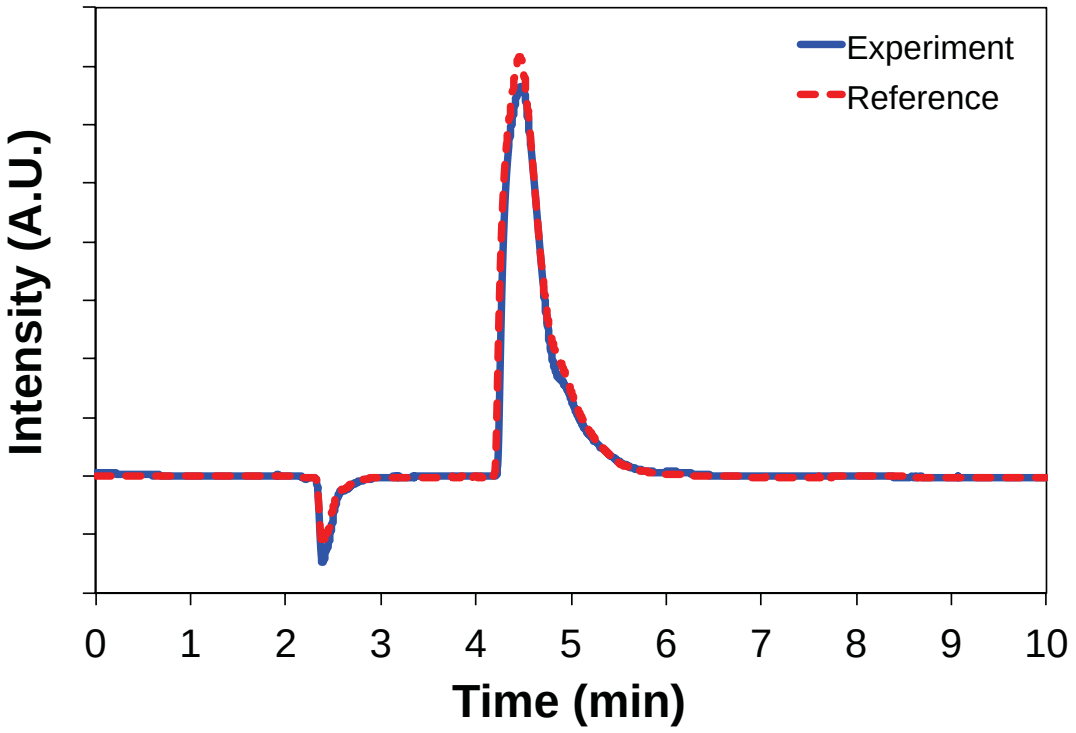

Fig. S17. Chromatogram of lidocaine hydrochloride (**2**) produced using the system (solid blue line) compared to the commercial reference (dashed red line).

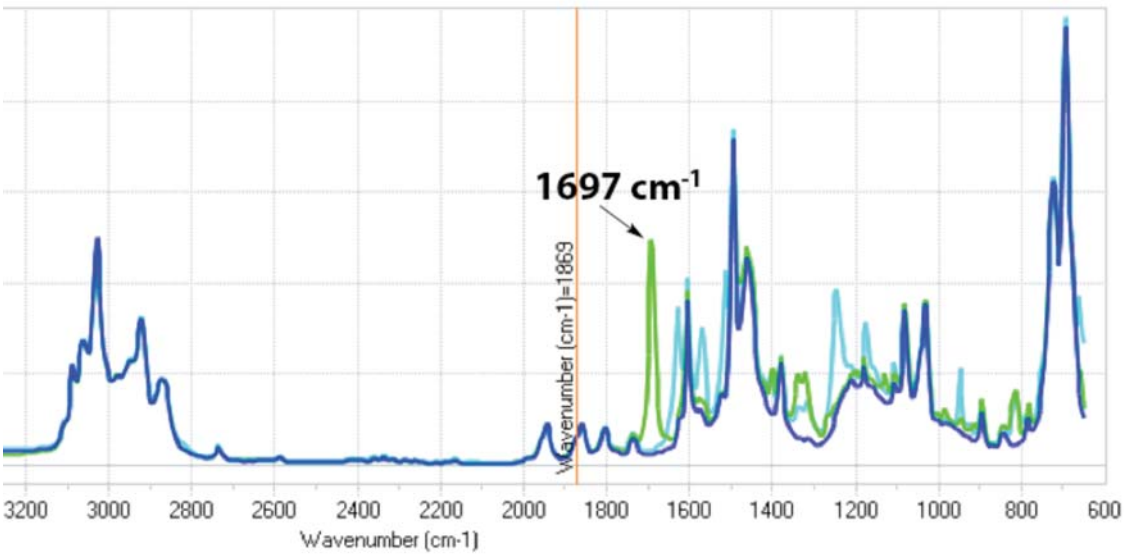

Fig. S18. IR spectral library for diazepam in toluene. Solutions of 2-methylamino-5-chlorobenzophenone (light blue) and diazepam (green) in toluene (dark blue) were utilized as standards for the IR library. The characteristic peak at 1697 cm^{-1} (ν_{CO}) was used to monitor the reaction. Ethyl acetate (dark blue) was more efficient for the extraction of diazepam, but partially masked the characteristic peak of diazepam (green) at 1697 cm^{-1}.

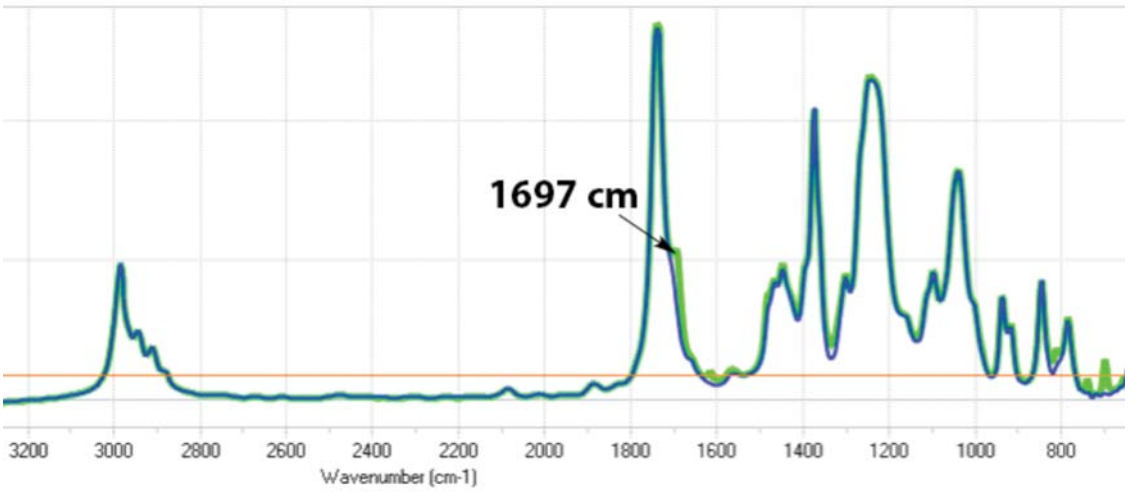

Fig. S19. IR spectral library for diazepam in ethyl acetate.

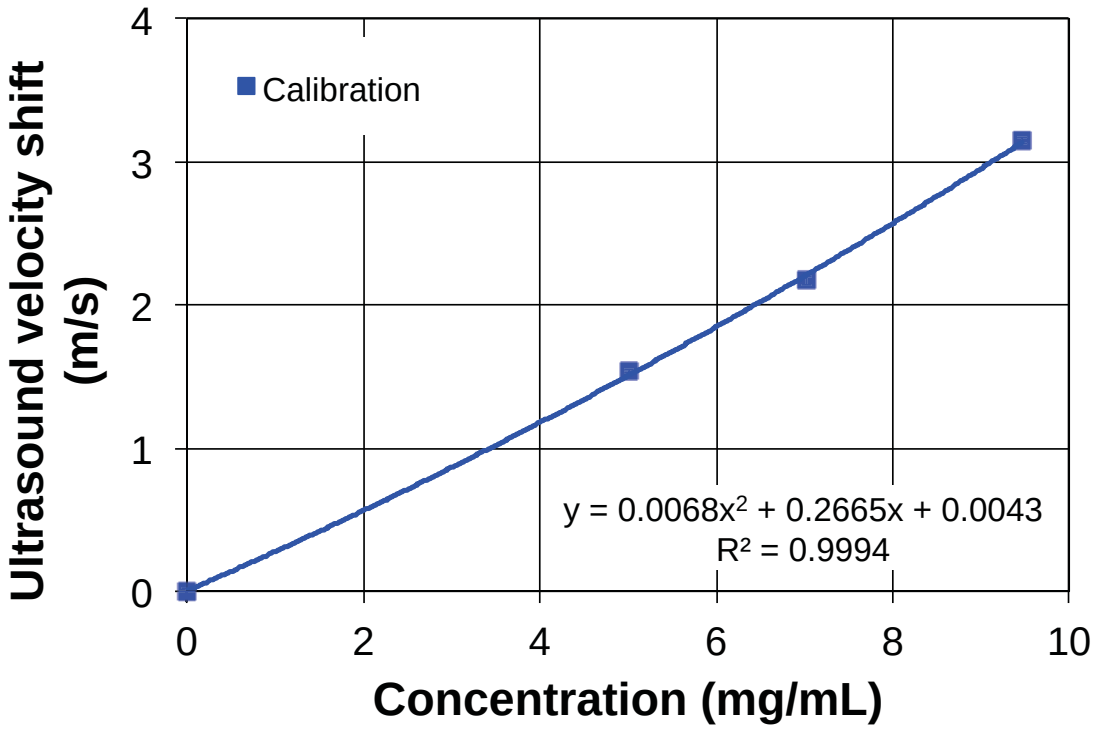

Fig. S20. Standard curve of the ultrasonic velocity as a function of diazepam in ethanol. This curve was used to determine the concentration of diazepam (**3**) in the formulation tank.

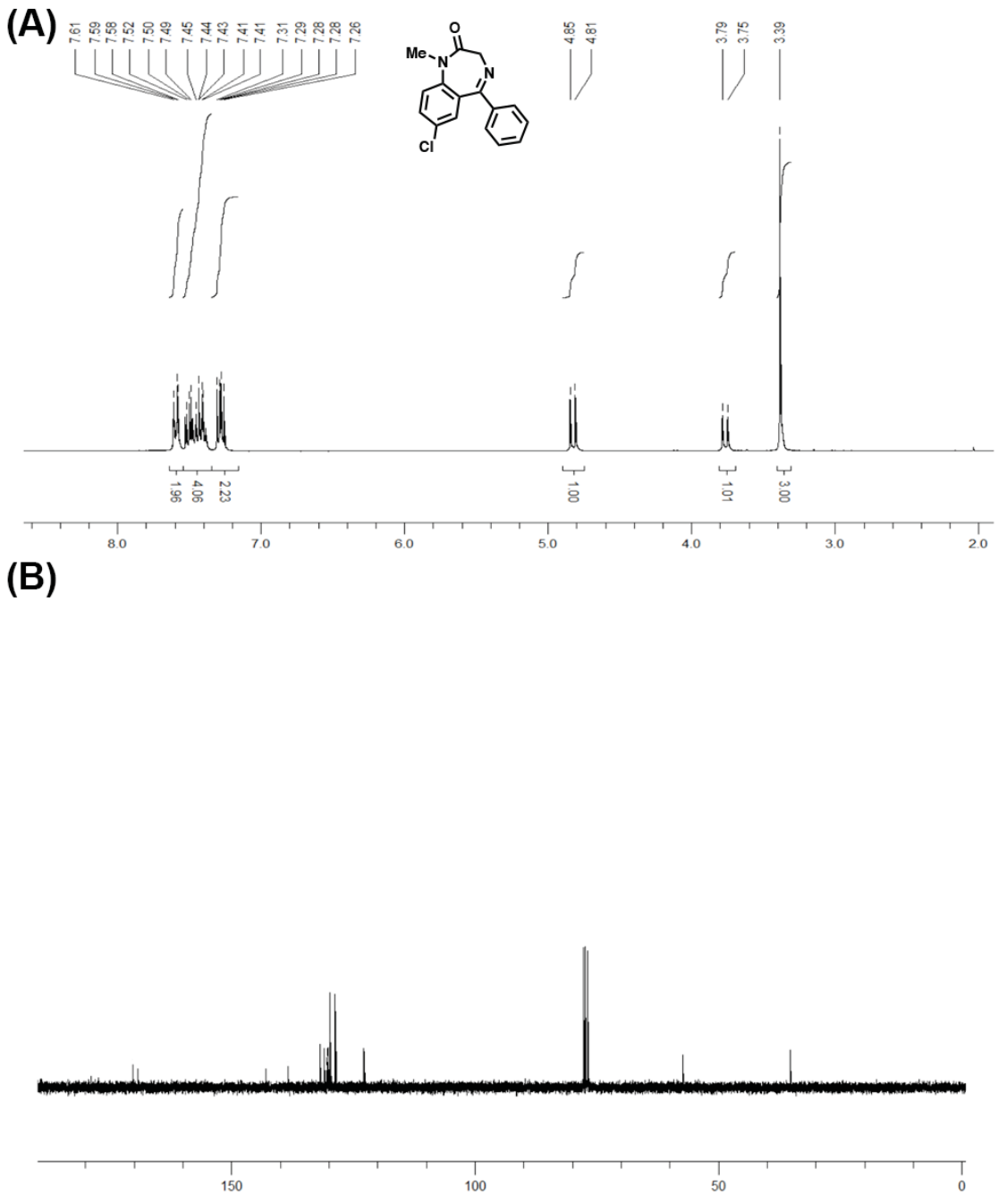

Fig. S21. (A) ^{1}H NMR (300 MHz, $CDCl_3$) and (B) ^{13}C NMR (75 MHz, $CDCl_3$) spectra of crude diazepam obtained from the upstream unit. Diazepam hydrochloride was first neutralized with aqueous ammonia, filtered and then dried prior to running the NMR experiments.

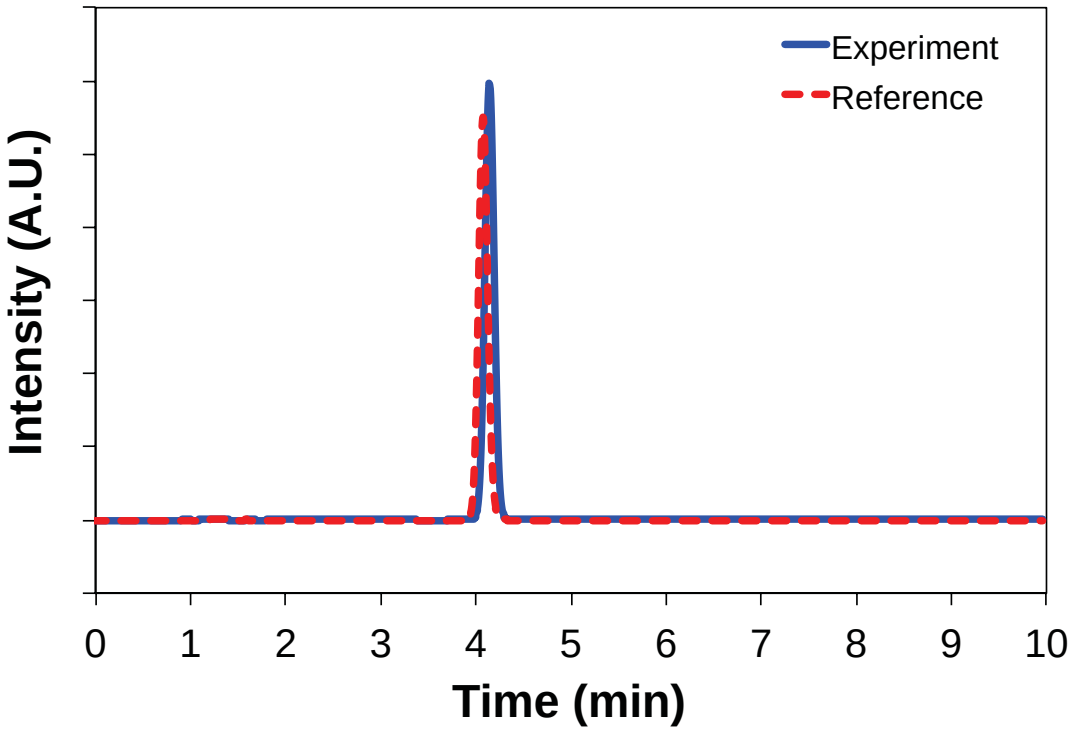

Fig. S22. Chromatogram of diazepam (**3**) produced using the system (solid blue line) compared to the commercially available reference (dashed red line).

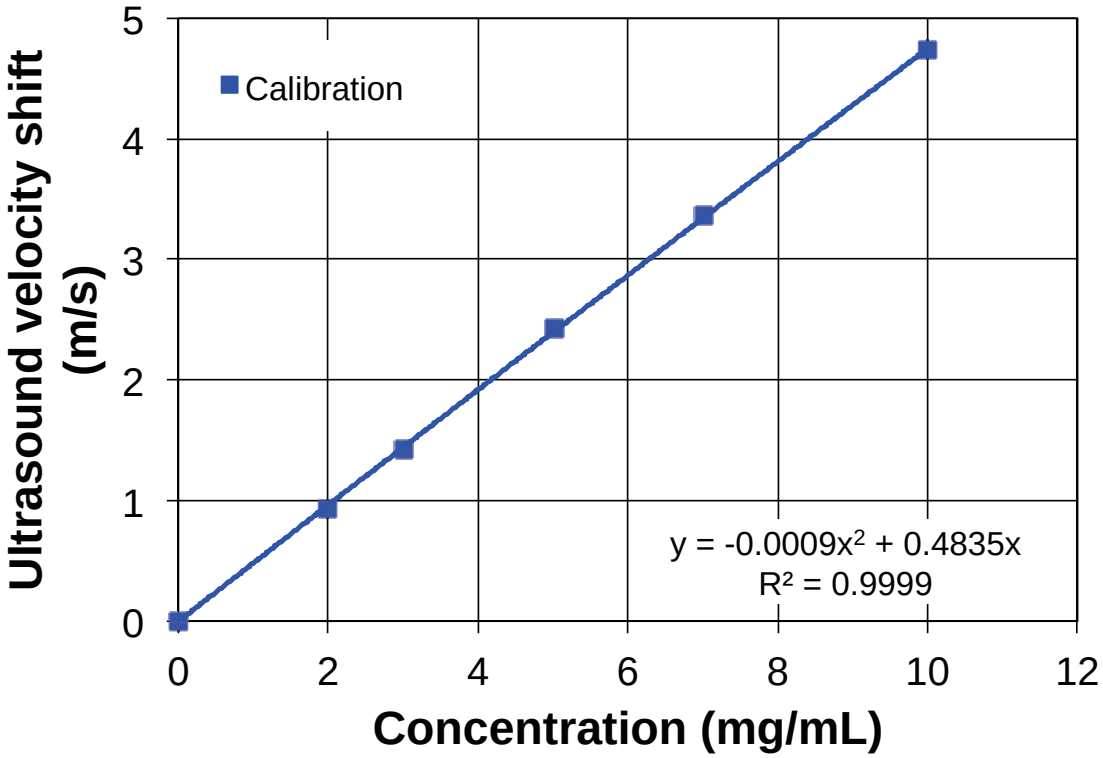

Fig S23. Standard curve of the ultrasonic velocity as a function of fluoxetine hydrochloride in water. This curve was used to determine the concentration of fluoxetine hydrochloride (**4**) in the formulation tank.

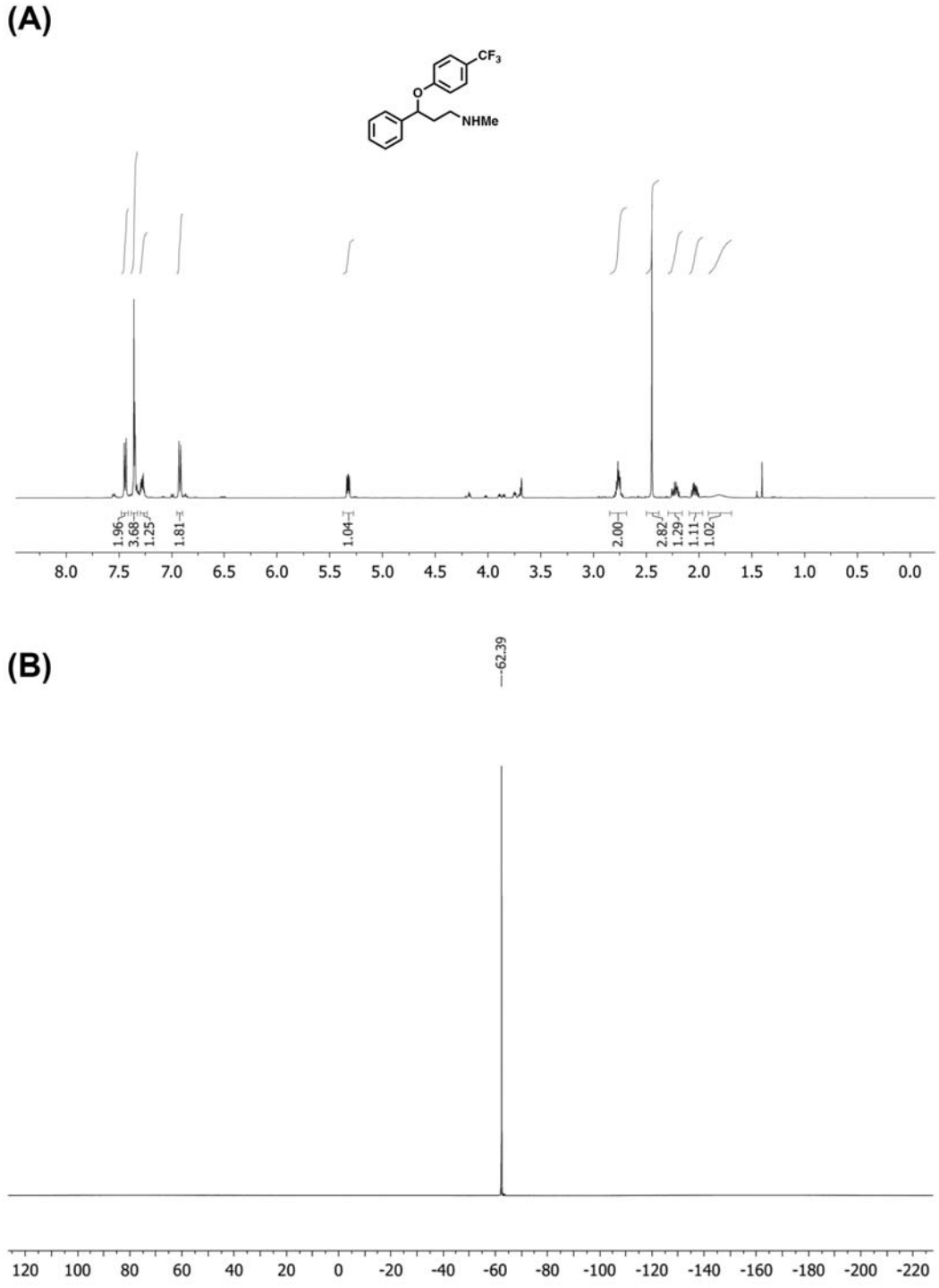

Fig. S24. (A) ^{1}H NMR (500 MHz, $CDCl_3$) and (B) ^{19}F NMR (282 MHz, $CDCl_3$, ref $CF_3C_6H_5$) spectra of fluoxetine obtained from the upstream after the extraction module (water/TBME). The sample was concentrated under reduced pressure prior to running the NMR experiment.

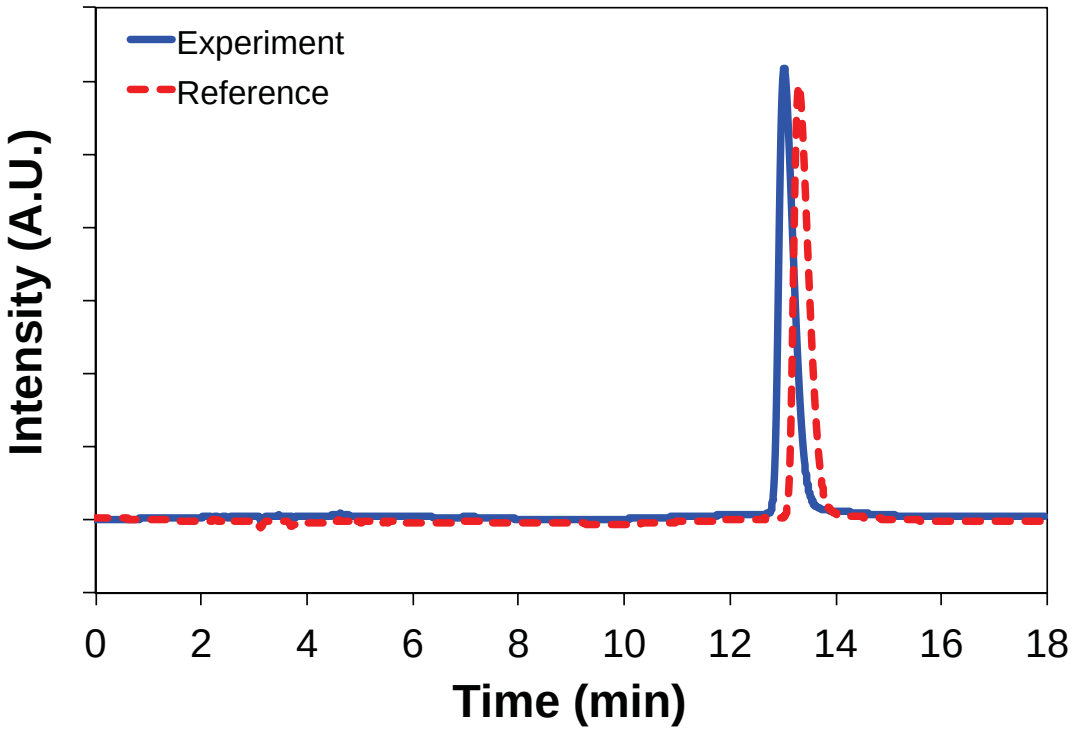

Fig. S25. Chromatogram of fluoxetine hydrochloride (**4**) produced using the system (solid blue line) compared to the commercial reference (dashed red line).

Table S1.
Drug product liquid formulations.

API	Concentration (mg/mL)	Excipients	Stability Tested (Days)
Diphenhydramine HCl	2.5	Water	32
Lidocaine HCl	20	Water + 2% NaOH = 4% sodium carboxymethylcellulose (added after production)	31
Diazepam	1	19% ethanol, 81% Water (vol:vol)	31
Fluoxetine HCl	4	Water	31

Table S2.
List of reagents and products for Fig. 2.

Stream	Target API
1	diphenhydramine HCl
2	lidocaine HCl
3	diazepam
4	fluoxetine HCl

Production of diphenhydramine hydrochloride (1)

Stream	Reagents/Solvents
5	2-dimethylaminoethanol
6	chlorodiphenylmethane
7	NaOH aqueous solution (3M)
8	hexanes
9	water
10	HCl/ Et_2O

Production of lidocaine hydrochloride (2)

Stream	Reagents/Solvents
11	2,6-xylidine (1.43 M in NMP)
12	chloroacetyl chloride
13	*N*-methyl-2-pyrrolidone (NMP)
14	Et_2NH (3.0 eq.), KOH (1.2 eq.) in MeOH/H_2O
15	hexanes
16	sat. NaCl/ NH_4Cl
17	HCl/ Et_2O

Production of diazepam (3)

Stream	Reagents/Solvents
18	5-chloro-2-(methylamino)benzophenone (1M in NMP)
19	bromoacetyl chloride
20	*N*-methyl-2-pyrrolidone (NMP)
21	ammonia solution (3.5 M in MeOH:H_2O, 9:1 mixture)
22	20% NaCl aqueous solution
23	ethyl acetate
24	HCl aqueous solution (4M)
25	NH_3/H_2O

Production of fluoxetine hydrochloride (4)

Stream	Reagents/Solvents
26	3-chloropropiophenone in toluene
27	DIBAL in toluene
28	4 M HCl
29	4 M HCl
30	$MeNH_2$ aqueous solution
31	NaCl solution
32	THF
33	4-fluorobenzotrifluoride in anhydrous DMSO
34	KO*t*Bu and 18-crown-6 in DMSO
35	water
36	TBME
37	HCl/Et_2O

Table S3.

Process times for the four APIs.

		Process time (hours)			
		Diphenhydramine hydrochloride	**Lidocaine hydrochloride**	**Diazepam**	**Fluoxetine hydrochloride**
	Upstream synthesis[1]	0.8	1.8	0.7	1.3
Downstream Processes[2]	**Precipitation**	5.5	9.0	24.0	36.0
	Upstream Filtration	1.5	1.5	1.5	1.5
	Holding tank	0.5	0.1	0.1	0.1
	Crystallizer 1	1.9	2.5	2.8	2.8
	Downstream Filtration 1	1.5	2.5	4.5	1.5
	Crystallizer 2	-	-	-	2.8
	Downstream Filtration 2	-	-	-	1.5
	Formulation	0.5	0.3	0.3	0.3
	Total cycle time	12.2	17.7	33.8	47.7

[1] This refers to the time for each synthesis to reach steady state, estimated to be three residence times of the sequential reactions.

[2] For the downstream processing (i.e. from precipitation to formulation), these residence times have accounted for the transfer of solvents, solutions, and suspensions as well as temperature equilibration.

References and Notes

1. C. Badman, B. L. Trout, Achieving continuous manufacturing. May 20-21, 2014 Continuous Manufacturing Symposium. *J. Pharm. Sci.* **104**, 779–780 (2015). Medline doi:10.1002/jps.24246

2. I. R. Baxendale, R. D. Braatz, B. K. Hodnett, K. F. Jensen, M. D. Johnson, P. Sharratt, J. P. Sherlock, A. J. Florence, Achieving continuous manufacturing: Technologies and approaches for synthesis, workup, and isolation of drug substance. May 20-21, 2014 Continuous Manufacturing Symposium. *J. Pharm. Sci.* **104**, 781–791 (2015). Medline doi:10.1002/jps.24252

3. S. Byrn, M. Futran, H. Thomas, E. Jayjock, N. Maron, R. F. Meyer, A. S. Myerson, M. P. Thien, B. L. Trout, Achieving continuous manufacturing for final dosage formation: Challenges and how to meet them. May 20-21, 2014 Continuous Manufacturing Symposium. *J. Pharm. Sci.* **104**, 792–802 (2015). Medline doi:10.1002/jps.24247

4. R. F. Service, The synthesis machine. *Science* **347**, 1190–1193 (2015). Medline doi:10.1126/science.347.6227.1190

5. S. Mascia, P. L. Heider, H. Zhang, R. Lakerveld, B. Benyahia, P. I. Barton, R. D. Braatz, C. L. Cooney, J. M. Evans, T. F. Jamison, K. F. Jensen, A. S. Myerson, B. L. Trout, End-to-end continuous manufacturing of pharmaceuticals: Integrated synthesis, purification, and final dosage formation. *Angew. Chem. Int. Ed.* **52**, 12359–12363 (2013). Medline doi:10.1002/anie.201305429

6. Food and Drug Administration, *Strategic Plan for Preventing and Mitigating Drug Shortages* (October 2013; www.fda.gov/downloads/Drugs/DrugSafety/DrugShortages/UCM372566.pdf).

7. L. Malet-Sanz, F. Susanne, Continuous flow synthesis. A pharma perspective. *J. Med. Chem.* **55**, 4062–4098 (2012). Medline doi:10.1021/jm2006029

8. D. Webb, T. F. Jamison, Continuous flow multi-step organic synthesis. *Chem. Sci.* **1**, 675–680 (2010). doi:10.1039/c0sc00381f

9. R. L. Hartman, J. P. McMullen, K. F. Jensen, Deciding whether to go with the flow: Evaluating the merits of flow reactors for synthesis. *Angew. Chem. Int. Ed.* **50**, 7502–7519 (2011). Medline doi:10.1002/anie.201004637

10. V. Hessel, Novel process windows - gate to maximizing process intensification via flow chemistry. *Chem. Eng. Technol.* **32**, 1655–1681 (2009). doi:10.1002/ceat.200900474

11. R. J. Ingham, C. Battilocchio, D. E. Fitzpatrick, E. Sliwinski, J. M. Hawkins, S. V. Ley, A systems approach towards an intelligent and self-controlling platform for integrated continuous reaction sequences. *Angew. Chem. Int. Ed.* **54**, 144–148 (2015). Medline doi:10.1002/anie.201409356

12. B. Gutmann, D. Cantillo, C. O. Kappe, Continuous-flow technology—a tool for the safe manufacturing of active pharmaceutical ingredients. *Angew. Chem. Int. Ed.* **54**, 6688–6728 (2015). Medline doi:10.1002/anie.201409318

13. M. Baumann, I. R. Baxendale, The synthesis of active pharmaceutical ingredients (APIs) using continuous flow chemistry. *Beilstein J. Org. Chem.* **11**, 1194–1219 (2015). Medline doi:10.3762/bjoc.11.134

14. F. Lévesque, P. H. Seeberger, Continuous-flow synthesis of the anti-malaria drug artemisinin. *Angew. Chem. Int. Ed.* **51**, 1706–1709 (2012). Medline doi:10.1002/anie.201107446

15. M. D. Hopkin, I. R. Baxendale, S. V. Ley, An expeditious synthesis of imatinib and analogues utilising flow chemistry methods. *Org. Biomol. Chem.* **11**, 1822–1839 (2013). Medline doi:10.1039/C2OB27002A

16. C. A. Correia, K. Gilmore, D. T. McQuade, P. H. Seeberger, A concise flow synthesis of efavirenz. *Angew. Chem. Int. Ed.* **54**, 4945–4948 (2015). Medline doi:10.1002/anie.201411728

17. M. Viviano, T. N. Glasnov, B. Reichart, G. Tekautz, C. O. Kappe, A scalable two-step continuous flow synthesis of nabumetone and related 4-aryl-2-butanones. *Org. Process Res. Dev.* **15**, 858–870 (2011). doi:10.1021/op2001047

18. P. Zhang, M. G. Russell, T. F. Jamison, Continuous flow total synthesis of rufinamide. *Org. Process Res. Dev.* **18**, 1567–1570 (2014). doi:10.1021/op500166n

19. D. Ghislieri, K. Gilmore, P. H. Seeberger, Chemical assembly systems: Layered control for divergent, continuous, multistep syntheses of active pharmaceutical ingredients. *Angew. Chem. Int. Ed.* **54**, 678–682 (2015). Medline

20. P. R. D. Murray, D. L. Browne, J. C. Pastre, C. Butters, D. Guthrie, S. V. Ley, Continuous flow-processing of organometallic reagents using an advanced peristaltic pumping system and the telescoped flow synthesis of (*E*/*Z*)-tamoxifen. *Org. Process Res. Dev.* **17**, 1192–1208 (2013). doi:10.1021/op4001548

21. P. L. Heider, S. C. Born, S. Basak, B. Benyahia, R. Lakerveld, H. Zhang, R. Hogan, L. Buchbinder, A. Wolfe, S. Mascia, J. M. B. Evans, T. F. Jamison, K. F. Jensen, Development of a multi-step synthesis and workup sequence for an integrated, continuous manufacturing process of a pharmaceutical. *Org. Process Res. Dev.* **18**, 402–409 (2014). doi:10.1021/op400294z

22. Materials and methods are available as supplementary materials on *Science* Online.

23. D. J. am Ende, in *Chemical Engineering in the Pharmaceutical Industry*, D. J. am Ende, Ed. (Wiley, NJ, 2011), chap. 1.

24. A. Adamo, P. L. Heider, N. Weeranoppanant, K. F. Jensen, Membrane-based, liquid-liquid separator with integrated pressure control. *Ind. Eng. Chem. Res.* **52**, 10802–10808 (2013). doi:10.1021/ie401180t

25. C. F. Carter, H. Lange, S. V. Ley, I. R. Baxendale, B. Wittkamp, J. G. Goode, N. L. Gaunt, ReactIR flow cell: A new analytical tool for continuous flow chemical processing. *Org. Process Res. Dev.* **14**, 393–404 (2010). doi:10.1021/op900305v

26. G. Rieveschl, Dialkylaminoalkyl benzhydryl ethers and salts thereof, U.S. Patent 2,421,714A, 3 June 1947.

27. S. Y. Wong, J. Chen, L. E. Forte, A. S. Myerson, Compact crystallization, filtration, and drying for the production of active pharmaceutical ingredients. *Org. Process Res. Dev.* **17**, 684–692 (2013). doi:10.1021/op400011s

28. USP (U.S. Pharmacopeia), Diphenhydramine hydrochloride capsules. *Monograph* **34**, 2597 (2014).

29. T. J. Reilly, The preparation of lidocaine. *J. Chem. Educ.* **76**, 1557 (1999). doi:10.1021/ed076p1557

30. N. M. Loefgren, B. J. Lundqvist, Alkyl glycinanilides, U.S. Patent 2,441,498, 11 May 1948.

31. USP (U.S. Pharmacopeia), Lidocaine hydrochloride. *Monograph* **37**, 3552–3553 (2014).

32. T. Sugasawa, M. Adachi, T. Toyoda, K. Sasakura, A new simple synthesis of 1,4-benzodiazepines. *J. Heterocycl. Chem.* **16**, 445–448 (1979). doi:10.1002/jhet.5570160306

33. USP (U.S. Pharmacopeia), Diazepam. *Monograph* **37**, 2580–2581 (2014).

34. B. Ahmed-Omer, A. J. Sanderson, Preparation of fluoxetine by multiple flow processing steps. *Org. Biomol. Chem.* **9**, 3854–3862 (2011). Medline doi:10.1039/c0ob00906g

35. R. L. Hartman, J. R. Naber, N. Zaborenko, S. L. Buchwald, K. F. Jensen, Overcoming the challenges of solid bridging and constriction during Pd-catalyzed C-N bond formation in microreactors. *Org. Process Res. Dev.* **14**, 1347–1357 (2010). doi:10.1021/op100154d

36. USP (U.S. Pharmacopeia), Fluoxetine hydrochloride. *Monograph* **37**, 3035–3036 (2014).

37. Food and Drug Administration, *FDA Perspective on Continuous Manufacturing*, (February 2013; www.fda.gov/downloads/AboutFDA/CentersOffices/OfficeofMedicalProductsandTobacco/CDER/UCM341197.pdf).

38. S. L. Lee, T. F. O'Connor, X. Yang, C. N. Cruz, S. Chatterjee, R. D. Madurawe, C. M. V. Moore, L. X. Yu, J. Woodcock, Modernizing pharmaceutical manufacturing: From batch to continuous production. *J. Pharm. Innov.* **10**, 191–199 (2015). doi:10.1007/s12247-015-9215-8

39. S. D. Schaber, D. I. Gerogiorgis, R. Ramachandran, J. M. B. Evans, P. I. Barton, B. L. Trout, Economic analysis of integrated continuous and batch pharmaceutical manufacturing: A case study. *Ind. Eng. Chem. Res.* **50**, 10083–10092 (2011). doi:10.1021/ie2006752

40. T. Stelzer, D. Pertig, J. Ulrich, Ultrasonic crystallization monitoring technique for simultaneous in-line measurement of liquid and solid phase. *J. Cryst. Growth* **362**, 71–76 (2013). doi:10.1016/j.jcrysgro.2011.11.027

41. J. G. Kralj, H. R. Sahoo, K. F. Jensen, Integrated continuous microfluidic liquid-liquid extraction. *Lab Chip* **7**, 256–263 (2007). Medline doi:10.1039/B610888A

42. B. G. Lipták, Ed., *Instrument Engineers' Handbook, Process Control* (Butterworth-Heinemann, ed. 3, 1995).

43. W. M. Deen, *Analysis of Transport Phenomena* (Oxford Univ. Press, ed. 2, 2012).